HHS Public Access

Author manuscript

*ACS Appl Mater Interfaces*. Author manuscript; available in PMC 2024 April 15.

Published in final edited form as:

*ACS Appl Mater Interfaces*. 2019 August 28; 11(34): 30518–30533. doi:10.1021/acsami.9b07353.

# Bioprinting of a Cell-Laden Conductive Hydrogel Composite

**Andrew R. Spencer**[†], **Ehsan Shirzaei Sani**[‡], **Jonathan R. Soucy**[†], **Carolyn C. Corbet**[§], **Asel Primbetova**[†,‖], **Ryan A. Koppes**[†], **Nasim Annabi**[*,‡,⊥,#]

[†]Department of Chemical Engineering, Northeastern University, Boston, Massachusetts 02115, United States

[‡]Chemical and Biomolecular Engineering Department, University of California–Los Angeles, Los Angeles, California 90095, United States

[§]Department of Bioengineering, Northeastern University, Boston, Massachusetts 02115, United States

[‖]School of Biomedical Engineering, University of British Columbia, Vancouver, British Columbia V6T 1Z2, Canada

[⊥]Biomaterials Innovation Research Center, Brigham and Women's Hospital, Harvard Medical School, Cambridge, Massachusetts 02139, United States

[#]Center for Minimally Invasive Therapeutics (C-MIT), California NanoSystems Institute (CNSI), University of California–Los Angeles, Los Angeles, California 90095, United States

## Abstract

Bioprinting has gained significant attention for creating biomimetic tissue constructs with potential to be used in biomedical applications such as drug screening or regenerative medicine. Ideally, biomaterials used for three-dimensional (3D) bioprinting should match the mechanical, hydrostatic, bioelectric, and physicochemical properties of the native tissues. However, many materials with these tissue-like properties are not compatible with printing techniques without modifying their compositions. In addition, integration of cell-laden biomaterials with bioprinting methodologies that preserve their physicochemical properties remains a challenge. In this work, a biocompatible conductive hydrogel composed of gelatin methacryloyl (GelMA) and poly(3,4-ethylenedioxythiophene):poly(styrenesulfonate) (PEDOT:PSS) was synthesized and bioprinted

[*]**Corresponding Author:** nannabi@ucla.edu.

Author Contributions

A.R.S., R.A.K., and N.A. conceived the project. A.R.S. ran EIS on hydrogel samples. A.R.S. and C.C.C. completed tensile mechanical testing and swelling experiments. E.S.S. performed SEM work. E.S.S. and A.R.S. performed in vivo degradation studies. E.S.S. performed H&E and immunofluorescent staining and imaging. A.R.S. completed rheological characterization of bioinks and support baths. A.R.S. characterized the printability and resolution of the bioinks with the FRESH support baths. A.R.S., J.R.S., and A.P completed in vitro cell culture experiments with C2C12 myoblasts. The manuscript was written through contributions of all authors. All authors have given approval to the final version of the manuscript.

Supporting Information

The Supporting Information is available free of charge on the ACS Publications website at DOI: 10.1021/acsami.9b07353. (Figure S1) Printing of GelMA/PEDOT:PSS bioinks at 15 °C onto a glass slide, (Figure S2) optimization of printing for bioinks containing various concentrations of PEDOT:PSS and at various applied pressures, (Figure S3) wet-spinning of C2C12-laden composite hydrogels, (Figure S4) immunofluorescent staining of subcutaneously implanted hydrogels, and (Figure S5) live/dead images of C2C12 cells bioprinted with 7% GelMA/0.3% PEDOT:PSS into support bath at various exposure times (PDF)

The authors declare no competing financial interest.

to form complex, 3D cell-laden structures. The biofabricated conductive hydrogels were formed by an initial cross-linking step of the PEDOT:PSS with bivalent calcium ions and a secondary photopolymerization step with visible light to cross-link the GelMA component. These modifications enabled tuning the mechanical properties of the hydrogels, with Young's moduli ranging from ~40–150 kPa, as well as tunable conductivity by varying the concentration of PEDOT:PSS. In addition, the hydrogels degraded in vivo with no substantial inflammatory responses as demonstrated by haematoxylin and eosin (H&E) and immunofluorescent staining of subcutaneously implanted samples in Wistar rats. The parameters for forming a slurry of microgel particles to support 3D bioprinting of the engineered cell-laden hydrogel were optimized to form constructs with improved resolution. High cytocompatibility and cell spreading were demonstrated in both wet-spinning and 3D bioprinting of cell-laden hydrogels with the new conductive hydrogel-based bioink and printing methodology. The synergy of an advanced fabrication method and conductive hydrogel presented here is promising for engineering complex conductive and cell-laden structures.

## Graphical Abstract

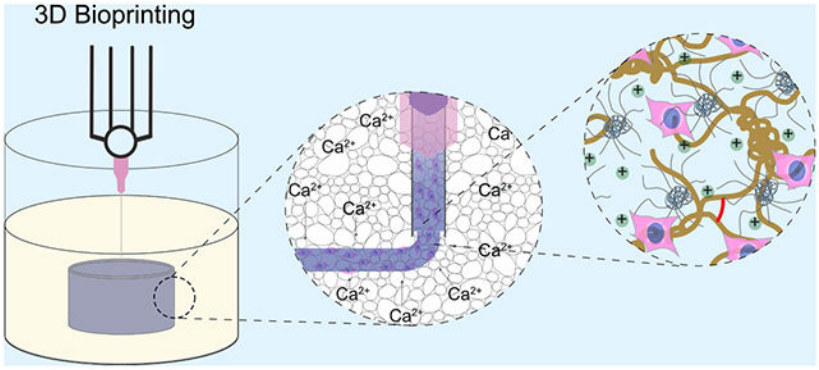


### Keywords

electroconductive; hydrogel; composite; conductive polymer; bioprinting

## 1. INTRODUCTION

Bioprinting is emerging as a promising method for forming three-dimensional (3D) tissue-like structures in vitro with biomimetic microarchitecture.[1] Advances in these methods may also allow fabrication of full-scale tissue de novo from a patient's own stem cells[2] and eliminate concerns with transplantation therapy, including competition for transplant sources and donor-host incompatibility.[3] Toward these advances, a large number of bioinks, synthesized from an array of materials (i.e., fibrin, silk, hyaluronic acid, and collagen) and possessing a number of functionalities (i.e., growth factor loading, phage DNA, and conductivity), have been demonstrated in the literature and are commercially available.[4] However, there remain several obstacles that must be overcome before full-scale, functional tissues and organs can be bioprinted.

Currently, a major limitation of extrusion bioprinting is that biomaterials that have shown promise in evoking strong cellular responses, such as those with relatively low mechanical stiffness and tissue-specific chemical composition (e.g., hydrogels), are often precluded from traditional bioprinting methods due to low structural stability following printing, resulting from low viscosity or slow cross-linking kinetics.[5] Approaches to impart existing biomaterials with printability include the addition of rheology modifiers, such as cellulose nanofibers[6,7] or silicate nanoparticles.[7,8] These additives usually result in highly viscous, shear-thinning bioinks that can be printed onto solid substrates, since their high viscosity arrests the flow of the ink and prevents collapse of the structure before cross-linking. However, the addition of these materials also affects the mechanical stiffness of the cross-linked hydrogels,[9,10] which can reduce cellular spreading and elongation within the scaffolds.[11] Further, an increase in viscosity of the bioink makes their mixing with cells more difficult, as it can introduce air bubbles into the ink and expose cells to high shear stresses, reducing viability and altering cellular phenotype.[12] Silicate nanoparticles have proven utility in engineering hard tissues, such as bone, due to their osteoinductive properties.[9] Cellulose-based hydrogels have shown promise as wound healing materials[13] and thus may have a place as an additive for bioprinting skin tissues.[14] However, the benefits of using these nanomaterials for regenerating other tissues are unclear.

In addition to the mechanical and biological properties of bioprinted tissue constructs, conductivity is important for excitable tissues such as cardiac,[15] skeletal,[16] and smooth muscle,[17] as well as neural tissues.[18] The incorporation of conductive materials has been proposed to bridge the insulating pore walls of cross-linked hydrogels, thereby coupling electrically disconnected cells.[19] When exposed to electrical stimulation, the signals are propagated through the construct evenly and uniformly stimulate cellularized constructs.[19,20] Furthermore, mimicking the mesoscale fibrous architecture found in skeletal muscle and neural tissues may be critical to recapitulate the function of native tissues. Fibrous architectures can be easily formed using wet-spinning and bioprinting techniques and thus have potential to be employed for generating these tissues in vitro.[21] Conductive nanomaterials, such as gold,[22] carbon nanotubes,[23] and graphene,[24] have been incorporated into 3D printable hydrogels to render the printed structures conductive. For example, a blend of gelatin methacryloyl (GelMA) and alginate mixed with gold nanorods was used for 3D printing cardiac tissue.[22] The alginate was added as a sacrificial material that enabled printing with a coaxial nozzle flowing aqueous calcium chloride in the sheath, and the gold nanorods imparted the hydrogel with conductivity. Cardiomyocytes printed in the gold nanorod-containing hydrogels exhibited improved contraction rate and expression of cardiac markers compared to controls, which was attributed to the gold nanorods creating conductive bridges throughout the matrix and promoting electrical signal propagation. In another study, a polyurethane-graphene composite hydrogel was used for 3D printing and differentiating neural stem cells.[24] Even at very low graphene loadings (25 ppm), oxygen metabolism and neural differentiation of the stem cells were significantly enhanced. However, to date, the constructs printed with conductive bioink lack complex geometries, and the conductive additives have little or no effect on the printability of the inks. In addition, inorganic nanomaterials such as graphene and carbon nanotubes have been shown to exhibit cytotoxicity, damage DNA, and/or produce reactive oxygen species (ROS), and

thus may be unsuitable for most bioprinting applications.[25] Therefore, new formulations of conductive bioinks as well as the adoption of strategies to print large and complex structures is required.

Transitioning from bioprinting onto solid substrates in air to support baths has enabled the fabrication of more complex and biomimetic structures.[26,27] For example, collagen has been extensively studied as a promising natural biomaterial for both two-dimensional (2D)[28] and 3D[29] cell cultures due to its abundance in native tissues, cell adhesiveness, and biodegradability. However, structures printed with collagen onto solid substrates lack complex geometry and have low resolution.[30,31] The use of a gelatin microparticle slurry enabled printing complex structures with collagen at low concentrations (<10 mg $mL^{-1}$), such as a bifurcating tube or femur.[26] Consequently, the use of support baths relaxes the rheological requirements for bioinks and can enable printing of low viscosity solutions, which inherently reduces the shear stresses on cells during printing. Therefore, instead of significantly modifying a biomaterial composition to enable printability, it may be more advantageous to adapt novel bioprinting methodologies with minor compositional adjustments to print biomimetic tissue constructs.

Recently, we reported on the synthesis and characterization of a photo-cross-linkable, electroconductive GelMA/PEDOT:PSS hydrogel that could be used to encapsulate mammalian cells with high cytocompatibility.[32] Due to the precise spatial and temporal control over polymerization, highly tunable physical properties, and opportunity to control their 2D and 3D architecture, photo-cross-linkable hydrogels are particularly well suited for biofabrication applications. Specifically, the rapid polymerization kinetics provide temporal control over the cross-linking, in contrast to traditional enzymatic or other chemical cross-linking methods.[33] In addition to control over the gelation process, GelMA hydrogel possesses cellular binding domains, arginine-glycine-aspartic acid (RGD), that further improve biological properties of this hydrogel.[34] Further, our previous study revealed that mixing of PEDOT:PSS into a GelMA hydrogel enhanced its conductivity and supported viability and spreading of C2C12 cells in 3D up to PEDOT:PSS loading of 0.1% (w/v).

In the work herein, we further modified our developed GelMA/PEDOT:PSS hydrogel and handling technique to form a new conductive material that can be used as a bioink for wet-spinning of cell-laden fibers and for 3D bioprinting. The hydrogel components were sequentially cross-linked in a series of physical and chemical cross-linking steps to form the composite hydrogels with robust mechanical and tunable electrical properties. A modified wet printing method was then used for generating complex 3D biomimetic structures with high resolution and printing fidelity. Both wet spinning and bioprinting methods were successful at maintaining viability and spreading of C2C12 myoblasts encapsulated in the fabricated hydrogel structures. The engineered GelMA/PEDOT:PSS bioink has potential to be used as a conductive bioink for printing excitable tissues with complex architectures.

## 2. EXPERIMENTAL SECTION

### 2.1. Materials.

Gelatin from porcine skin, methacrylic anhydride, Eosin Y disodium salt, triethanolamine (TEA), *N*-vinylcaprolactam (VC), anhydrous calcium chloride, and gold-coated glass slides with a titanium adhesive layer and 100 nm gold coating were purchased from Sigma-Aldrich (St. Louis, MO, USA). Dulbecco's modified phosphate buffered saline (DPBS) with no calcium or magnesium was purchased from GE Healthcare Life Sciences (Logan, Utah). PEDOT:PSS was in the form of an aqueous dispersion called Clevios PH 1000 and was purchased from Heraeus (Hanau, Germany). Calcein AM and ethidium homodimer-1 for live/dead assay and DAPI and Phalloidin conjugated to AlexaFluor 488 for actin/DAPI assay were purchased from Invitrogen (Carlsbad, CA). A LS1000 FocalSeal Xenon Light Source from Genzyme was used for photo-cross-linking of the hydrogels.

### 2.2. Preparation of GelMA/PEDOT:PSS Prepolymer Solutions.

Photo-cross-linkable GelMA prepolymer with ~80% methacryloyl functionalization degree was first synthesized using a previously reported procedure.[32,35] In brief, 10 g of gelatin from porcine skin was dissolved in 100 mL of DPBS at 60 °C. Once fully dissolved, 8 mL of methacrylic anhydride (Sigma) was added dropwise to the solution and allowed to homogenize. After 3 h of reaction, 300 mL of preheated DPBS at 60 °C was added to the solution to stop the reaction. This solution was then dialyzed against deionized (DI) water in dialysis tubing with a molecular weight cutoff (MWCO) of 12–14 kDa for 5 days, with DI water changed twice daily. After dialysis, the GelMA was lyophilized for 4 days to generate a fibrous white foam. GelMA solutions were prepared by dissolving appropriate amounts of the lyophilized GelMA in cell culture media with Eosin Y disodium salt (0.01% (w/v)), TEA (1.8% (w/v)), and VC (1.25% (w/v)) at 37 °C. Commercially available PEDOT:PSS solution (Clevios PH 1000) was sterile filtered (0.22 $\mu$m) to remove large aggregates. The concentration of the solution, after filtering, was found to be 1.05% (w/v) by drying and weighing. PEDOT:PSS was added to solutions of GelMA prepolymer to make the appropriate concentrations of the final volume in small volume increments with intermittent vortex mixing.

### 2.3. GelMA/PEDOT:PSS Hydrogel Formation and Characterization.

**2.3.1. Mechanical Testing.—**Tensile testing was performed using an Instron 5944 mechanical tester on rectangular gels. Hydrogel samples were formed by pouring 60 $\mu$L prepolymer solution into rectangular polydimethylsiloxane (PDMS) molds (13.0 mm L × 5.0 mm W × 0.82 mm H). The samples were placed in the refrigerator at 4 °C for 10 min and then submerged in calcium chloride solution or DPBS (control) at 4 °C for 10 min. The molds were removed from the cold solution, and the samples were then cross-linked with visible light (450–550 nm, 100 mW $cm^{-2}$) for 240 s on top and 240 s on bottom. The samples were removed from the molds and positioned between the grips of the instrument. Samples were pulled to failure at a strain rate of 1 mm $min^{-1}$. Young's modulus was taken as the slope of the linear portion of the curve from 0 to 10% strain.

**2.3.2. Electrochemical Impedance Spectroscopy (EIS).—**EIS measurements were performed at room temperature on a CH Instruments (Austin, TX, USA) electrochemical workstation. The apparatus was composed of two 12 × 12 mm glass slides coated with 100 nm of gold (Sigma-Aldrich). The electrodes were connected to copper wires with silver paste, and this connection was covered with epoxy resin to prevent tarnishing of the silver. Cylindrical hydrogels of 60 μL (6.0 mm D × 2.0 mm H) were swollen in ultrapure water for 16 h at 37 °C to remove the salt ions present in the hydrogels. The water was then replaced with fresh DI water twice. To ensure even cross-sectional areas of the hydrogel samples after swelling, circular sections of the gels were punched with a 0.6 cm biopsy punch and sandwiched between the gold-coated glass slides. A 0.65 mm PDMS spacer was placed around the gel to maintain a constant distance between the electrodes. The top electrode was then taped down on the spacer to maximize contact between the electrodes and the hydrogel. Measurements were recorded between 0.1 and 1000 Hz with an AC amplitude of ±10 mV.

**2.3.3. Swelling Ratio.—**Cylindrical samples of 60 μL volume (6.0 mm D × 2.0 mm H) were prepared and photo-cross-linked as described in section 2.3.1, briefly washed with ultrapure water to remove excess salt on the hydrogels, and lyophilized. Dry weights were recorded, and the samples were submerged in DI water and then placed into an oven at 37 °C. DI water was used instead of DPBS to prevent formation of calcium phosphate precipitates from calcium in the hydrogels and phosphate ions in DPBS. Samples were removed and weighed at different time points (1, 4, 8, 12, and 24 h). The swelling ratio was calculated following the equation:

$$\frac{(W_{\text{wet}} - W_{\text{dry}})}{W_{\text{dry}}} \times 100\% \quad (1)$$

where $W_{\text{dry}}$ is the weight after lyophilizing and $W_{\text{wet}}$ is after removal from DI water.

**2.3.4. Scanning Electron Microscopy (SEM).—**Fiber samples were prepared as described in section 2.4.4 without cells, soaked in ultrapure water (18.2 MΩ cm) for 24 h with three changes of the water and lyophilized using an Isotemp −80 °C freezer (Fisher Scientific, Hampton, NH) and a FreeZone 4.5 lyophilizer (Labconco, Kansas City, MO). Samples were then sectioned in half with a razor blade and sputter-coated with a Pt/Pd alloy. SEM images were obtained on a Hitachi S4800 SEM operating at 3.0 kV and 8 mm working distance.

## 2.4. Microfabricating GelMA/PEDOT:PSS Hydrogel Using Wetspinning and 3D Bioprinting.

**2.4.1. Preparation of Support Bath for 3D Bioprinting.—**The support bath was prepared as described previously[26] with some modification. Briefly, 6.75 g of gelatin from porcine skin was dissolved in 150 mL of 2% (w/v) $CaCl_2$ in DI water at 60 °C to make a solution of 4.5% (w/v) gelatin in a mason jar. The solution was covered and placed in a refrigerator at 4 °C overnight to solidify the gelatin. After this, 350 mL of 2% $CaCl_2$ was added to fill the jar, and the jar was capped with the gasket and blade from a commercial

blender (Oster SimpleBlend 10) and blended for 120 s. The resulting slurry was loaded into 50 mL centrifuge tubes and centrifuged at 10,000 rcf for 5 min. The supernatant was replaced with fresh 2% $CaCl_2$, mixed back into suspension, and centrifuged again. This process was repeated until no white foam remained at the top of the tube, indicating the complete removal of dissolved gelatin from the slurries. Support baths with different packing ratios were prepared by adding appropriate volumes of 2% $CaCl_2$ at 4 °C to make 1–2× dilutions and mixed.

**2.4.2. Rheological Characterization of Bioinks and Support Bath.—**A rheometer (Discovery Hybrid, TA Instruments, New Castle, DE) equipped with a cone plate (1.007°) with a gap size of 27 $\mu$m and a diameter of 40 mm was used to characterize the rheological properties of the bioinks. Prepolymer solutions were prepared as outlined in section 2.2 in cell culture media and were then pipetted onto the rheometer. Temperature was swept at 2 °C $min^{-1}$, and viscosity was determined as a function of temperature under a constant shear amplitude and rate of 1 Hz. Temperature was varied from 4 to 40 °C. For strain rate sweeps, the solutions were maintained at 25 °C, and shear rate was varied from 0.01 to 1000 $s^{-1}$.

For characterization of the support baths, more advanced rheology equipment was required to reduce noise during oscillatory stress sweeps. A rheometer (ARES G2, TA Instruments, New Castle, DE) equipped with a flat plate with a gap size of 150 $\mu$m and a diameter of 40 mm was used to characterize the rheological properties of the support bath slurries. The support baths were prepared as outlined in section 2.4.1 and loaded onto the rheometer before testing. The parallel plates of the rheometer were maintained at 4 °C for the tests. Oscillatory stress sweeps were performed at a constant angular frequency of 1 Hz.

**2.4.3. 3D Printing of GelMA/PEDOT:PSS and Fiber Diameter Measurements. —**Prepolymer solutions were prepared as outlined in section 2.2 and were allowed to cool to 25 °C in a 3 mL syringe affixed to a 30 gauge blunt end needle. Support baths with varied packing ratios were prepared and poured into a custom-made poly(methyl methacrylate) (PMMA) cube. The syringe was loaded onto an INKREDIBLE+ bioprinter printhead from Cellink and was maintained at 25 °C. Pressure was varied to change the flow rate (70–90 kPa) of the bioinks and printed into short cylinders with a layer height of 160 $\mu$m with a custom G-code. The printed structures were then exposed to light (450–550 nm) to cross-link for 80 s, carefully removed from the support bath with forceps, washed with warm DPBS, sectioned with a razor blade, and imaged with an inverted microscope (Primovert, Carl Zeiss, Inc.). The images were collected and analyzed with the ROI and Measure functions in ImageJ. Six images were measured per printing condition, and 60 fiber measurements were taken per image. Histograms were generated and analyzed using GraphPad Prism software.

**2.4.4. Cell Encapsulation in 3D Printed Hydrogels.—**C2C12 cells (ATCC CRL1772) were cultured under standard conditions (37 °C; 5% $CO_2$) with Dulbecco's modified eagle medium (DMEM) supplemented with 10% fetal bovine serum and 1% penicillin/streptomycin (Life Technologies).

7% GelMA/0.3% PEDOT:PSS hydrogel precursor solution was prepared as previously described (section 2.2) in cell culture media under sterile conditions. Cells were detached using trypsin-EDTA (0.25% v/v), centrifuged, and resuspended in the precursor solution at 10 million cells $mL^{-1}$. Cells were loaded into 3 mL syringes and connected to 30 gauge blunt end needles and loaded into the bioprinter. The bioprinter printhead was set to a temperature of 25 °C, and the pressure was set at 70 kPa for extrusion of the prepolymer solution. The support bath was prepared as outlined in section 2.4.1, and the gelatin bath at 1.6× dilution with 2% (w/v) calcium chloride at 4 °C was used. The structures were printed at an *X*–*Y* speed of 5–10 mm $s^{-1}$ into the bath and then exposed to light for 80 s to cross-link the GelMA before removing the structures from the bath and melting away excess gelatin particles by heating at 37 °C. The printed structures were washed with media, and the media was changed twice in the first 30 min to remove unreacted photoinitiator. Live/dead and actin/DAPI assays were performed on days 1, 3, 5, and 7. For live/dead, cells were stained with calcein AM (live) or ethidium homodimer-1 (dead) and incubated for 20 min. After staining, scaffolds were washed with DPBS three times and wells were filled with 400 μL of DPBS until the samples were imaged. For actin/DAPI assay, cells were fixed in 4% paraformaldehyde for 20 min and washed three times with DPBS with 5 min intervals between washes. This was followed by permeabilization with 0.1% Triton X-100 in DPBS for 20 min. Filamentous actin was stained with AlexaFluor 488 conjugated to Phalloidin (1:200) for 45 min and washed three times with DPBS, followed by staining of the cell nuclei with DAPI for 5 min and three washes with DPBS. Fluorescent images were obtained on an inverted microscope (Zeiss Axio Observer Z1). Cell viability and cell spreading were quantified using ImageJ software (NIH) from live/dead images and actin/DAPI images, respectively, according to previously published protocols.[36,37]

#### 2.4.5. Wet Spinning of GelMA/PEDOT:PSS to Form Cell-laden Fibers.—

To form cell-laden fibers, cells were mixed with prepolymer solutions as outlined in section 2.4.4, cell suspensions were loaded into syringes fit with 18 gauge blunt needles, injected into coagulation baths containing 2% (w/v) $CaCl_2$ in DI water at 4 °C, and cross-linked with light for 160 s in sterile conditions. Samples were cultured in 24 well plates with 400 μL of media. Media was changed twice in the first 30 min after cross-linking to remove unreacted photoinitiator and subsequently changed daily. Live/dead and actin/DAPI staining of bioprinted structures was performed as outlined in section 2.4.4.

### 2.5. In Vivo Biodegradation and Biocompatibility.

#### 2.5.1. Dorsal Subcutaneous Implantation of Hydrogels.—

The animal protocol was approved by the Institutional Animal Care and Use Committee (Protocol no. 15–1248R) at Northeastern University (Boston, MA, USA). Subcutaneous implantation of hydrogels in rats was performed as described previously.[38] Cylindrical samples were used for this study to simplify the evaluation of biodegradation and inflammatory response of the GelMA/PEDOT:PSS hydrogels as compared to the control GelMA hydrogels. Male Wistar rats (200–250 g) were purchased from Charles River Laboratories (Wilmington, MA, USA). Hydrogels (7% GelMA; 7% GelMA + 0.3% PEDOT:PSS, both cross-linked using 2% $CaCl_2$) were prepared under sterile conditions in cylindrical molds (2 × 6 mm disks), and their initial wet weights (day 0) were recorded. General anesthesia and analgesia were

induced by inhalation of isoflurane (2.5% (v/v)), followed by subcutaneous meloxicam administration (5 mg $kg^{-1}$). Next, 8 mm subcutaneous pockets were made through the posterior dorsal skin. Freshly prepared GelMA and GelMA/PEDOT:PSS hydrogels were then implanted into the subcutaneous pockets.

#### 2.5.2. Degradation Study, Histopathological Analysis, and Immunostaining.

—On days 7, 28, and 56 postimplantation, the animals were euthanized by $CO_2$ inhalation, and the samples were explanted for biodegradation and histopathological analysis. For biodegradation study, the samples were precisely cleaned to remove the adjacent tissue, and their weight was measured and compared to the initial weight. For immunohistological analysis, the samples with the surrounding tissue were fixed in 4% (v/v) paraformaldehyde overnight. Next, the samples were washed 3 times with DPBS and incubated at 4 °C in 30% sucrose solution overnight, followed by embedding in Optimal Cutting Temperature (OCT) compound and flash freezing with liquid nitrogen. The samples were then cryo-sectioned (10 $\mu$m) using a Leica Biosystems CM3050 S Research Cryostat machine. Hemotoxylin and Eosin (H&E) and immunofluorescent staining were performed as described previously.[38,39] For immunohistochemistry, samples were stained for normal and neo-plastic T cells (1:200 Anti-CD3 [SP7], ab16669, Abcam) and monocytes and macrophages (1:200, Anti-CD68, ab125212, Abcam) as primary antibodies, and Alexa Fluor 546-conjugated as secondary antibody (Invitrogen; A11034). Finally, samples were counterstained with DAPI (Invitrogen) and imaged using an inverted Axio Observer Z1 microscope (Carl Zeiss, Oberkochen, Germany).

### 2.6. Statistical Analysis.

All experiments were performed at least in triplicate, and data are presented as mean ± standard deviation (SD). Statistical analysis was performed in GraphPad Prism software. One-way ANOVA tests were performed to determine statistical significance, and P values less than 0.05 were considered as significant.

## 3. RESULTS AND DISCUSSION

### 3.1. Hydrogel Design and Synthesis.

To develop a highly biocompatible and conductive bioink, GelMA (Figure 1A) and PEDOT:PSS, which is a synthetic conducting polymer complex (Figure 1B), were physically, ionically, and covalently cross-linked together. Without any modification, mammalian gelatin (porcine, bovine, etc.) transitions from a viscous liquid to an elastic gel for a range of concentrations as temperature decreases,[40] while PEDOT:PSS forms a highly conductive cross-linked polyelectrolyte complex in an ionic solution containing multivalent cations.[41] Therefore, a composite of GelMA/PEDOT:PSS was partially cross-linked by injecting the liquid prepolymer into a bioprinting support bath containing aqueous calcium chloride at 4 °C (Figure 1C,D), which was due to the partial physical gelation of GelMA and ionic cross-linking of PEDOT:PSS. The physically cross-linked hydrogel was then further cross-linked covalently through photopolymerization of the methacryloyl groups on GelMA (Figure 1E), yielding a highly conductive and stable hydrogel.

### 3.2. Physical and Microstructural Characterization of GelMA/PEDOT:PSS Hydrogels.

Electrochemical impedance spectroscopy (EIS) was used to characterize the electrical properties of the GelMA/PEDOT:PSS composite hydrogels. As expected, while maintaining GelMA at 7% (w/v) and calcium chloride in DI water at 2% (w/v) concentrations, impedance decreased with increasing concentration of PEDOT:PSS (Figure 2A). In addition, the conductivity of the GelMA/PEDOT:PSS composite hydrogels did not change by increasing calcium chloride concentration from 0 to 3% w/v (Figure 2B). This was in contrast with previous studies showing that the presence of bivalent $Mg^{2+}$ or $Ca^{2+}$ ions in solution could enhance the conductivity of PEDOT:PSS hydrogels.[41] In our system, the hydrogels were swollen and sequentially rinsed in DI water before impedance testing. Therefore, $Ca^{2+}$ ions might diffuse out from the hydrogels or exchange with monovalent ion impurities in the DI water,[41] thereby bringing the conductivity back to that of hydrogels that were not cross-linked ionically. A similar phenomenon occurred for calcium-alginate hydrogels submerged in cell culture medium over the course of several days.[42] However, calcium ions are present in cell culture medium, thus prolonging the dissolution of alginate to days. In our experiment, ultrapure water was used and was almost completely devoid of calcium, which significantly accelerated the diffusion of calcium from the gels. Cross-linking the PSS with a higher molecular weight polycation, such as chitosan or polylysine, may combat this ion exchange after incubation in DI water so that conductivity may be enhanced with increasing concentration of the cross-linker. On the basis of the impedance curves, the conductivity of our hydrogels was similar to that of other conductive hydrogels that have been shown to improve electroactive tissue function.[22,43,44]

The elastic modulus of composite hydrogels was examined for the samples cross-linked with solutions of varying $CaCl_2$ concentrations. As expected, the introduction of the salt solution increased the stiffness of hydrogels containing PEDOT:PSS, while there was no statistical significance between the modulus of pristine GelMA hydrogels as the concentration of $CaCl_2$ changed. Specifically, for pristine GelMA hydrogels, the moduli were 120.0 ± 30.8 kPa for hydrogels submerged in DPBS and 113.8 ± 15.1 kPa for hydrogels submerged in 2% $CaCl_2$ (Figure 2C). The modulus of hydrogels containing 0.1% and 0.3% PEDOT:PSS submerged in DPBS were 79.1 ± 14.4 kPa and 40.9 ± 0.1 kPa, respectively, where the modulus of hydrogels containing 0.1% and 0.3% PEDOT:PSS submerged in cold, aqueous $CaCl_2$ were 141.6 ± 27.8 kPa and 80.0 ± 16.3 kPa, respectively. These data show that the $CaCl_2$ participated in the cross-linking of the hydrogel and enhanced its mechanical stiffness. In accordance with our previous results, hydrogel modulus decreased as PEDOT:PSS loading increased for hydrogels that were not cross-linked with $CaCl_2$, and this was attributed to reduced light penetration through the opaque hydrogels.[32] Interestingly, hydrogels with 0.1% PEDOT:PSS appeared to recover the mechanical strength of the hydrogels with 0% PEDOT:PSS when they were soaked in 2% $CaCl_2$ (NS), which could be attributed to the added cross-linking of PSS with calcium ions (Figure 2C). The modulus of hydrogels containing 0.3% PEDOT:PSS increased upon cross-linking with $CaCl_2$ but did not fully recover the stiffness of 0% PEDOT:PSS. There appears to be a linear correlation for the modulus of hydrogels and PEDOT:PSS concentration when the hydrogels are not cross-linked with $CaCl_2$, where modulus decreases linearly with PEDOT:PSS loading. However, the correlation for hydrogels that were cross-linked with $CaCl_2$ was not

linear, since the modulus of 0.3% PEDOT:PSS hydrogels decreased even when cross-linked with calcium. This indicates that the cross-linking of GelMA contributes to the modulus of the hydrogels more than the weaker ionic cross-linking of PSS. In addition, supporting this hypothesis is that the swelling ratio of the hydrogels, an indicator of the degree of cross-linking,[45] was increased with PEDOT:PSS loading (Figure 2D). Interestingly, compared to our previous GelMA/PEDOT:PSS hydrogel formulations that exhibited moduli in the range of ~8–10 kPa, changing the gelatin source from fish to porcine and cross-linking with calcium chloride increased the elastic moduli within the range of ~40–140 kPa. This 5-fold increase in stiffness can be attributed to the physical and ionic cross-linking of porcine GelMA and PEDOT:PSS, respectively, and to the use of a longer wavelength light for photopolymerization of GelMA. The absorption spectra of GelMA/PEDOT:PSS prepolymer solutions taken in our previous study showed lower absorbance in the 450–550 nm range than at 365 nm, suggesting that light in the 450–550 nm range may penetrate the samples better and more homogeneously cross-link the hydrogels than 365 nm light.[32] The dual cross-linked hydrogels presented here have stiffnesses that are slightly higher than the range of skeletal and cardiac muscle tissues (~10 kPa).[46,47] However, for many polymeric hydrogel systems, the stiffness can easily be tuned by changing the concentration of the polymer component, photoinitiator concentration, or exposure time. This is in contrast to thermoplastic polymer scaffolds, where the stiffness is not as easily modulated.[48] In contrast to other conductive bioinks, our formulations had relatively low stiffness (<0.2 MPa) and swelling ratio (<1300%), both of which may be beneficial in forming functional soft tissue. For example, in one study a conductive ink for 3D printing conductive implantable scaffolds with elastic moduli ranged from ~3 to ~17 MPa was introduced.[49] These constructs were made from poly(lactide-*co*-glycolide) mixed with graphene particles, and their high stiffness combined with cytotoxic organic solvents made them unsuitable for cell encapsulation. Another ink composed of poly(ethylene glycol) diacrylate (PEGDA) and carbon nanotubes had stiffness ranging from ~0.4 to ~1 MPa and was used for nerve regeneration.[50]

The relatively high stiffnesses of these bioinks might preclude them from successfully engineering soft tissues that develop most effectively on substrates with stiffnesses close to the native tissue.[51,52] Furthermore, the maximum swelling ratio of all hydrogel formulations tested herein occurred for the formulation with 7% GelMA and 0.3% PEDOT:PSS and was close to 1000% (Figure 2D). Interestingly, hydrogels containing 0.3% PEDOT:PSS very slightly deswell after 1 h (Figure 2D), which could indicate a slight loss of un-cross-linked material that leached from the hydrogel. However, there was no statistically significant difference between the swelling ratios at 1 h and those after. Highly hydrophilic inks for 3D printing exhibit extremely high swelling ratios, which can result in deformation of the printed construct, significant loss of resolution, and mechanical hysteresis.[53] For example, a modified degradable PEGDA hydrogel that was used for cell printing had water absorption between ~1900–3800% at 10% concentration.[54] Similarly, an elastic and conductive 3D printed ionic composite hydrogel exhibited swelling ratios up to 3500%, and structures that were printed with the composite deformed drastically upon swelling.[55] The relatively low swelling ratio and tunable stiffness of the conductive GelMA/PEDOT:PSS hydrogels presented here can make them more appropriate for bioprinting soft tissues.

SEM images of the hydrogels containing 7% (w/v) GelMA and 0.3% PEDOT:PSS, cross-linked with 2% (w/v) $CaCl_2$ (Figure 2E–G) showed smooth pore walls, possibly indicating lack of aggregation and good dispersion of the PEDOT:PSS in the hydrogel. This is in contrast to our previous study, in which large aggregates (~200 nm) were observed in the GelMA/PEDOT:PSS hydrogels.[32] The reduced aggregation observed herein could be due to the increased ionic strength of the prepolymer solutions attributed to sodium ions from Eosin Y disodium salt photoinitiator, as well as calcium ions that were used to cross-link the PEDOT:PSS. These ions can neutralize sulfonate groups on the PSS backbone and could mitigate its interaction with GelMA, thereby improving the dispersion of the polyelectrolyte in the hydrogels.

### 3.3. Rheological Characterization of GelMA/PEDOT:PSS for Use As a Conductive Bioink.

Characterization of the rheological properties of materials intended to be used as bioinks for printing tissues is important, as it can help researchers in anticipating the stability of the printed structures and the potential impacts on encapsulated cells during extrusion printing. Due to the presence of porcine gelatin, the GelMA/PEDOT:PSS composite is temperature-sensitive. Therefore, the response of the bioinks, containing various concentrations of PEDOT:PSS, to changes in temperature were evaluated. Here, the viscosity of inks containing PEDOT:PSS was higher than pristine GelMA at all temperatures tested (4–40 °C) (Figure 3A) and the viscosity increased with increasing PEDOT:PSS concentration. Lastly, GelMA/PEDOT:PSS composites responded to changes in temperature similarly to GelMA, with decreasing viscosity at high temperatures and higher viscosity at lower temperatures (Figure 3A). On the basis of these data, a constant temperature of 25 °C was maintained for bioprinting cell-laden conductive hydrogels. Specifically, at 25 °C the prepolymer solutions had sufficiently low viscosity and thus mitigated the effects of shear stress on cells. Furthermore, this temperature did not induce local melting of the gelatin particles in the support bath as the prepolymer was extruded, which was observed when printing the prepolymer at 37 °C.

In addition to testing the composite bioink's response to temperature, its shear-thinning properties were also assessed. Here, the strain sweep experiment demonstrated that all hydrogel formulations exhibited shear-thinning properties, but the effect was enhanced for formulations containing PEDOT:PSS (Figure 3B). The effect of shear rate on viscosity of the solutions became more linear as the loading of PEDOT:PSS increased. This behavior may be explained by weak and reversible interactions of PEDOT:PSS nanoparticles with the GelMA chains, which were reduced under higher shear rates but recovered as shear was decreased. Nanocomposites of silicate nanoparticles or nanoclay and charged polymers exhibited similar shear thinning properties due to electrostatic interactions between charges on the polymer and the dispersed nanoparticles.[8] These strong shear-thinning properties enabled printing of structures containing PEDOT:PSS onto solid substrates as shown in Figure S1, where filaments extruded with PEDOT:PSS-containing inks maintained their shape and did not flow into adjacent filaments. Polymer solutions with weak shear-thinning properties, such as alginate, expose cells to increasing shear at elevated shear rate, thus reducing cell viability and altering cell phenotype.[12] Shear-thinning fluids, such as partially cross-linked alginate, exhibit the same amount of shear stress at increasing shear

rates, which may improve viability of cells under shear.[56] In the context of the GelMA/PEDOT:PSS bioink presented here, the interactions of PEDOT:PSS with GelMA created a viscous, shear-thinning ink that may protect cells from membrane disruption during shear stresses and preserve cell viability. Despite this improvement in shear-thinning behavior, complex structures could not be printed onto glass slides as the ink viscosity was not high enough after extrusion to hold a structure between adjacent layers. Therefore, a support bath was used to print complex structures.

### 3.4. Characterization of Modified Support Bath for 3D Bioprinting.

In the past decade, 3D printing of soft biomimetic structures into self-healing support baths has gained significant attention due to the level of technical simplicity it provides for 3D printing of soft materials into complex shapes.[26,27,57] Direct printing into a biocompatible support bath enhances the stability of structures that are unstable with low-viscosity inks in air and enables post-processing to stabilize the printed structure. Here, the GelMA/PEDOT:PSS composite required the use of a support bath, since its viscosity at room temperature (25 °C) (Figure 3A) was insufficient for printing large structures onto a solid substrate. At lower temperatures (~15 °C), all prepolymer solutions were highly viscous and could be extruded directly onto glass; however, the printed structures were well-resolved only for ~1 layer of printing (Figure S1). Printing into the cold (4 °C) calcium-containing support bath served as the primary ionic cross-linking step of the PSS chains and thermal gelling of the GelMA chains (Figure 4A,B). After printing, the structure in the support bath was exposed to visible light to cross-link the GelMA prepolymer (Figure 4C). Once the printed structure was fully cross-linked, the gelatin particles in the support bath were melted away at 37 °C. This method is known as freeform reversible embedding of suspended hydrogels (FRESH).[26]

The effect of decreased packing on the printability of our hydrogels was studied. The FRESH printing method is characterized by gelatin microgels packed into a support bath to yield a slurry like a Bingham plastic, which act as a solid until a threshold stress, above which it behaves like a liquid.[26] This allows for uninterrupted nozzle movement through the support bath as material is deposited and support for the deposited material as the structure is formed. In addition, the nozzle movements lead to the appearance of “spurs” in the printed filaments, which are proposed to help bind the discrete filaments together to form the larger printed structure.[26] However, the spurs reduce the fidelity and resolution of the printed structures for a mean particle diameter of 55.3 ± 2 $\mu$m and a 150 $\mu$m nozzle diameter. Since the particle size was ~1/3 the size of the nozzle and the support bath was fully packed, the spurs caused high variability in the filament diameter. The occurrence of spurs was a result of stressed gelatin particles disturbing the extruded filaments and creating defects.[26]

Therefore, to improve the resolution of FRESH bioprinting, the packing of the tightly packed slurry was loosened simply by diluting it with the calcium-containing aqueous solvent (Figure 4D). Oscillatory stress sweeps of the microgel medium showed that the storage modulus of the slurries remained high until a threshold yield stress (Figure 4E). As expected, the storage modulus and yield stress of the diluted baths were lower than that of the fully packed bath. Decreasing the packing of the slurry beyond a dilution factor of 1.6×

yielded a fluid that was too loosely packed to support structures (Figure 4F). At dilutions beyond this, namely 1.8× and 2×, the extruded filaments that were formed began to sink toward the bottom of the bath, resulting in a continuous but axially disconnected fiber. In addition, for bioink compositions containing <0.3% PEDOT:PSS, clearly defined filaments were not visible in cross sections of the printed structures (Figure 4F). Consequently, bioinks containing 0.3% PEDOT:PSS were used for remaining bioprinting experiments. At support bath dilutions as low as 1.2×, impressions of filaments started to become visible in lateral cross sections of the printed structures (Figure 4G). As the packing was decreased to 1.4× dilution, the spurs became less frequent and were almost completely absent at 1.6× dilution, the condition that yielded smooth stacked fibers (Figure 4G, right). Before photo-cross-linking, the printed structures containing 7% GelMA and 0.3% PEDOT:PSS could be easily torn apart with tweezers and lacked structural integrity. However, after light exposure, the printed structures were bonded together and maintained their macrostructural and mechanical integrity and could be removed from the support bath by melting away the gelatin particles at 37 °C. This indicates that the GelMA in adjacent extruded fibers chemically bonded together in the photo-cross-linking reaction and provides that contact between the filaments is crucial in forming a stable printed structure.

Controlling the diameter of the printed filaments can be accomplished by adjusting the nozzle diameter, flow rate of the bioink, and printhead speed. However, for simplicity, the printhead speed was maintained at 10 mm $s^{-1}$ and a 30 gauge needled was used (ID = 160 $\mu$m). The effect of flow rate on the width of the fibers was assessed by varying the pressure between 70 and 90 kPa (Figure 4H). Histograms of the measurements showed Gaussian-like distribution. Applied pressures of 70, 80, and 90 kPa at 1.4× dilution provided fiber diameters centered at 120.1 ± 36.02 $\mu$m, 141.1 ± 36.29 $\mu$m, and 142.4 ± 43.76 $\mu$m, respectively. When the dilution factor was increased to 1.6×, pressures of 70, 80, and 90 kPa provided filament diameters of 121.4 ± 33.27 $\mu$m, 139.0 ± 24.55 $\mu$m, and 136.5 ± 35.5 $\mu$m, respectively. Filaments printed at 1.2× faintly showed impressions of straight fibers with an abundance of defects and were not measured. While there was an appreciable increase in the mean diameter of fibers when increasing the applied pressure from 70 to 80 kPa (~20 $\mu$m) at 1.4× and 1.6× dilutions, there was a much smaller increase by raising the pressure from 80 to 90 kPa (~1 $\mu$m). This is likely because, at flow rates greater than 80 kPa, the extruded filaments become more tightly crowded in the $Z$-direction and thus shift outward in the $X$–$Y$ direction. In agreement with this hypothesis, there was an increase in the thickness of the walls of printed structures when the pressure was increased in this range (Figure S2). Significant differences in the diameter of fibers were not observed when decreasing the packing ratio from 1.4× dilution to 1.6× dilution (Figure 4H), thereby confirming that the decreased packing reduces the occurrence of spurs and enhances printing fidelity with no effect on the diameter of the printed filaments.

### 3.5. 3D Bioprinting and Wet Spinning of Cell-Laden Structures.

Here, our developed GelMA/PEDOT:PSS bioinks were used to form cell-laden 3D conductive constructs by 3D printing in a reduced packing support bath. In addition, a wet-spinning technique was used to make fibrous structures based on GelMA/PEDOT:PSS as a validation of the biocompatibility of the processing technique. C2C12 murine myoblasts,

as a model cell, were mixed with the prepolymer solutions, injected into aqueous $CaCl_2$ at 4 °C, and photo-polymerized with visible light (Figure S3A–C). Bivalent calcium ions rapidly interacted with the anionic PSS chains and caused immediate cross-linking at the point of injection. The original structure was reinforced by exposing the fiber to visible light to further cross-link the GelMA biopolymer. Injection of GelMA prepolymer solutions containing PEDOT:PSS concentration lower than 0.3% did not produce stable fibers, indicating that the PEDOT:PSS concentration was crucial to the formation of fibers. Similarly, it was found that fibers could be formed by injecting the GelMA/PEDOT:PSS dispersion into aqueous calcium chloride at room temperature. However, these fibers were extremely weak and difficult to handle, indicating that the temperature-mediated cross-linking of GelMA was crucial to the formation of mechanically stable fibrous structures.

Results of our previous study on a cell-laden GelMA/PEDOT:PSS composite hydrogel showed that high concentrations (>0.1% w/v) of PEDOT:PSS significantly reduced viability of C2C12 myoblasts encapsulated in the hydrogels.[32] This may be attributed to the fact that PSS is 2.5× more abundant than PEDOT by weight, and that PSS strongly interacts with guanidinium groups on arginine in gelatin backbone,[58] which limits interaction of integrins with the arginine-glycine-aspartic acid (RGD) groups and reduces cell attachment. Here, we sought to investigate if increasing the concentration of salt in the hydrogel would mitigate the interaction of PSS with arginine, thus improving cellular attachment, spreading, and long-term survival. Quantification of live/dead and actin/DAPI assays (Figure S3) showed the high viability and spreading of C2C12s in the wetspun fibers. Altogether, these results indicated that the interaction of PSS chains with arginine was mitigated and the hydrogel and fabrication technique supported cell attachment and spreading in 3D structures.

The high biocompatibility of GelMA/PEDOT:PSS composite hydrogel cross-linked with calcium, as demonstrated by wet-spinning, suggest the promise of this material as conductive bioink for printing complex cell-laden structures with the newly developed modified FRESH printing method (Figure 5). The conductive bioink and modified FRESH printing method were first used to print a complex, hollow “buckyball” structure that mimicked the structure of the carbon fullerene molecule (Figure 5A–C). This structure is particularly complex because it contains a high frequency of hollow areas and diagonal lines, which cannot be easily printed with traditional bioprinting methods. The frequent arches and hollow areas would likely require sequential printing of support material at every layer, which appreciably increases the time required to print and can reduce the fidelity of the structure. Here, printing of the buckyball structure was complete in ~7 min. In addition, we confirmed the ability to print complex biological structures by printing a complete left heart with the aorta (Figure 5D–F). The model of the structure was downloaded from the NIH 3D print exchange (3dprint.nih.gov) and was edited to remove artifacts and to facilitate 3D printing. The GelMA/PEDOT:PSS bioink and printing methodology presented here could be used to print complex electroactive tissue structures on demand from medical scans. Although the complexity of the printed structures was high, they were relatively weak and flattened when removed from aqueous media. This is expected for such large hollow constructs. In one study, the structural integrity of large bioprinted constructs was addressed by printing thermoplastic support material made of polycaprolactone (PCL).[59] However, PCL degrades relatively slowly and might present a barrier to tissue ingrowth

for implanted constructs. In addition, the bulk printing resolution for the large constructs is fair, and some artifacts can be observed in Figure 5B,C and Figure 5E,F. These artifacts were partially a result of the weak cross-linking of PEDOT:PSS, which did not create a fully stabilized structure before polymerizing GelMA with light. During printing these large complex structures, the movements of the needle skewed the printed filaments and created artifacts. This could be improved by incorporating a material that cross-links strongly in the presence of calcium, such as alginate[26,42] or gellan gum.[60]

It was expected that viability and spreading of C2C12 myoblasts in bioprinted constructs would be similar to the results of wet-spinning, as the fabrication process was nearly identical, with a few minor differences. For bioprinting experiments, the cell-laden prepolymer solution was extruded through a smaller diameter needle (160 $\mu$m) at 25 °C into the support bath containing aqueous $CaCl_2$ and gelatin micro-particles at 4 °C. We anticipated the most important difference would be the smaller diameter of the needle, which could expose the cells to shear stress during the printing process, especially with highly viscous bioinks. For example, in a bioink composed of alginate, GelMA, and gold nanorods, cardiac cells extruded through nozzles of 200 $\mu$m inner diameter exhibited lower viability (<70%) at flow rates greater than 10 $\mu$L $min^{-1}$ at which shear stress was increased.[22] However, myoblasts printed into cylindrical ring structures (Figure S2) with 160 $\mu$m in this study exhibited high viability (>95%) and spreading at all days tested (Figure 5G–L). The data shown in Figure 5G–L are representative of cell viability and spreading at multiple focal planes in the center and periphery of printed constructs. Since the cell-laden constructs were 2 fibers thick as per G-code instructions, and the average diameter of fibers printed with 7% GelMA/0.3% PEDOT:PSS at 70 kPa was ~120 $\mu$m (Figure 4G), the construct thickness was estimated at ~240 $\mu$m. Media was present in both the inside and outside of the cylindrical constructs, so the farthest a cell should be from nutrients in the media is ~120 $\mu$m. This is below the limit of diffusion in tissues[61] and should not create necrotic cores. Myoblasts in the bioprinted constructs exhibit a rounded morphology at day 1 (Figure 5G,J) but appeared to elongate as the construct degrades over the 7 days of culture (Figure 5H,K). In addition, the cells appeared to be fusing at day 7 for both bioprinted constructs (Figure 5K, inset) and in wetspun fibers (Figure S3). This is a prerequisite to myogenesis, in which myoblasts undergo fusion to form multinucleated cells, ultimately forming elongated myotubes.[62,63] Existing literature has shown that forming myotubes from myoblasts cultured in 3D hydrogels is best achieved when the constructs are exposed to either cyclic mechanical stimulation[59] or continuous tension.[63] Electrical stimulation has also been shown to improve the elongation of myotubes for C2C12 and primary muscle progenitor cells encapsulated in 3D hydrogels.[64] These methods can be used to further differentiate the myoblasts in our hydrogel and form mature muscle constructs.

### 3.6. Subcutaneous Implantation of Composite Hydrogels.

Here, the in vivo biodegradation and biocompatibility of GelMA/PEDOT:PSS hydrogels was assessed using a rat subcutaneous implantation model. Visual examination of the explanted hydrogels revealed that the physical size of the hydrogels shrank over the course of the experiment (Figure 6A), indicating possible degradation via enzymatic cleavage of the GelMA backbone. In addition, significant host tissue infiltration was observed within the

samples. This observation was consistent across implanted samples over the course of the experiment (Figure 6B). The average degradation of the explanted hydrogels by weight increased from 27.13 ± 0.97% and 46.46 ± 3.40% for pure GelMA hydrogels and GelMA/PEDOT:PSS hydrogels, respectively, at day 7 to 71.19 ± 9.28% and 69.62 ± 11.4% at day 28 (Figure 6B). However, the biodegradation percentage decreased to 48.81 ± 3.28% and 61.05 ± 5.51% for GelMA and GelMA/PEDOT:PSS hydrogels, respectively, on day 56 postimplantation, which may be the result of new tissue ingrowth within the gels (Figure 6B). In agreement with this result, histopathological and immunofluorescence analyses (Figure 6C–F) showed significant hydrogel degradation from day 7 to day 56. The border between the hydrogel and tissues were not clear at day 56, and cells stained with DAPI can be observed in the hydrogel structures, indicating cell penetration and tissue ingrowth. We previously characterized in vitro degradation for our original GelMA/PEDOT:PSS hydrogels, which showed that the control and composite hydrogels degraded hydrolytically over 14 days.[32] We anticipate that the gelatin-based hydrogels presented in the previous work and here would degrade more quickly in vivo in the presence of host collagenase. Hematoxylin and eosin (H&E) staining indicated that the samples were progressively biodegraded and replaced by newly formed tissue for both GelMA and composite GelMA/PEDOT:PSS hydrogels (Figure 6C,D). These results indicated that neither the pristine GelMA nor hydrogels containing PEDOT:PSS elicited strong inflammatory responses. Interestingly, when PEDOT:PSS was previously used as a conductor for a neural cuff electrode, H&E staining of peripheral nerve cross sections revealed that there was epineural fibrosis and mild endoneurial degeneration for control polyimide cuffs and cuffs containing PEDOT:PSS and PEG hydrogel.[65] This was only mitigated in the presence of the immunosuppressant cyclosporine A. However, these aggressive inflammatory responses were not observed for GelMA/PEDOT:PSS hydrogels which were ionically cross-linked with calcium. The inflammatory responses of GelMA/PEDOT:PSS composite hydrogels and control GelMA hydrogels were assessed by immunofluorescent staining. Fluorescent images showed minor infiltration of lymphocytes (anti-CD3) with no macrophage (anti-CD68, red) infiltration at day 7 (Figure 6E). The results were similar for day 28 (Figure S4). After 56 days of implantation, there was no detectable sign of lymphocytes or macrophages in both control GelMA and GelMA/PEDOT:PSS samples (Figure 6F). These results suggest that our conductive bioinks were biodegradable and biocompatible. Further studies would be required to determine the effect of elastic modulus and electroactive properties of the printed constructs in vivo.

## 4. CONCLUSIONS

This study presents the development of a biocompatible and conductive bioink for 3D bioprinting of complex cell-laden structures. The bioink formulation was shown to exhibit tunable physical properties, such as mechanical stiffness and conductivity, as well as high biocompatibility both in vitro and in vivo. The improved biocompatibility of the hydrogel formulation with the highest concentration of PEDOT:PSS was likely a result of ionic cross-linking of the PEDOT:PSS nanoparticles, as well as improved light penetration through the opaque samples due to the use of a longer wavelength light source. Ionic cross-linking mitigated the interaction of PSS with the gelatin chain and improved cell

attachment, while visible light was able to fully cross-link the GelMA and improve viability. Modification of a novel bioprinting method utilizing a microgel support bath improved the fidelity of printed structures. Specifically, the reduced packing of the microgels preserved the technical simplicity of printing complex structures with the engineered conductive and cell-friendly bioink, while reducing the occurrence of spurs in the extruded filaments. High viability was achieved when printing with a 30 gauge (160 $\mu$m) nozzle, likely due to the temperature-dependent viscosity and shear thinning properties of the conductive composite ink. This enabled printing of filaments resolved as low as 120 $\mu$m. Although the size of cell-laden extruded filaments was ~120–140 $\mu$m and cell alignment was not observed, the reduction in spurs resulted in smoother filaments with few projections that deviated from the printing direction. Efforts to reduce the size of the filaments even further (<100 $\mu$m) may help in aligning different cell types, such as cardiomyocytes.[66,67] In contrast to other rheological additives that are used to improve printability, increased loading of PEDOT:PSS improved both conductivity and printing fidelity while maintaining high viability for cells encapsulated in the 3D structures. In this study, however, only small (~10–15 layer) cell-laden constructs could be printed with high viability for 7% GelMA/0.3% PEDOT:PSS hydrogels due to the short exposure times (80 s) required to cross-link. The longer exposure times (240 s) required for large constructs reduced viability of cells in the network (Figure S5). These long exposure times were likely required due to the opaque color of the composite gels, which was found to reduce light penetration through the gels in our previous study.[32] Using a transparent conducting material, such as the bio-ionic liquid,[68] may help overcome this obstacle. Despite these limitations, the developed conductive bioink and printing method presented here have potential for fabricating complex cell-laden and electroactive structures. Such structures may be useful in applications involving cell transplantation for regenerating electroactive tissues, where the conductivity of the implant improves bioelectric function of the tissue during the regeneration process. For example, cardiac progenitor cells can be printed into patterns mimicking the fibrous architecture of the heart and implanted into infarcted cardiac tissue. The conductivity of the hydrogel may improve cardiac function in vivo[69] while the cardiac progenitor cells can differentiate into mature cardiomyocytes and regenerate cardiac muscle tissue.[70]

## Supplementary Material

Refer to Web version on PubMed Central for supplementary material.

## ACKNOWLEDGMENTS

N.A. acknowledges the support from the American Heart Association (AHA, 16SDG31280010) and the National Institutes of Health (R01-EB023052; R01HL140618). R.K. and A.S. acknowledge the support from Northeastern University and the startup fund provided by the Department of Chemical Engineering, College of Engineering, at Northeastern University. The authors also acknowledge Dr. Su-Ryon Shin for assistance with electrochemical impedance spectroscopy. J.R.S. acknowledges the predoctoral fellowship support from the American Heart Association Grant (19PRE34430181).

## REFERENCES

(1). Murphy SV; Atala A 3D Bioprinting of Tissues and Organs. Nat. Biotechnol 2014, 32 (8), 773–785. [PubMed: 25093879]

(2). Gu Q; Tomaskovic-Crook E; Wallace GG; Crook JM 3D Bioprinting Human Induced Pluripotent Stem Cell Constructs for In Situ Cell Proliferation and Successive Multilineage Differentiation. Adv. Healthcare Mater 2017, 6 (17), 1–11.

(3). Radenkovic D; Solouk A; Seifalian A Personalized Development of Human Organs Using 3D Printing Technology. Med. Hypotheses 2016, 87, 30–33. [PubMed: 26826637]

(4). Gungor-Ozkerim PS; Inci I; Zhang YS; Khademhosseini A; Dokmeci MR Bioinks for 3D Bioprinting: An Overview. Biomater. Sci 2018, 6 (5), 915–946. [PubMed: 29492503]

(5). Yeh Y; Highley CB; Ouyang L; Burdick JA 3D Printing of Photocurable Poly (Glycerol Sebacate) Elastomers. Biofabrication 2016, 8 (4), 1–10.

(6). Shin S; Park S; Park M; Jeong E; Na K; Youn HJ; Hyun J Cellulose Nanofibers for the Enhancement of Printability of Low Viscosity Gelatin Derivatives. BioResources 2017, 12 (2), 2941–2954.

(7). Jungst T; Smolan W; Schacht K; Scheibel T; Groll J Strategies and Molecular Design Criteria for 3D Printable Hydrogels. Chem. Rev 2016, 116 (3), 1496–1539. [PubMed: 26492834]

(8). Chimene D; Peak CW; Gentry JL; Carrow JK; Cross LM; Mondragon E; Cardoso GB; Kaunas R; Gaharwar AK Nanoengineered Ionic-Covalent Entanglement (NICE) Bioinks for 3D Bioprinting. ACS Appl. Mater. Interfaces 2018, 10 (12), 9957–9968. [PubMed: 29461795]

(9). Xavier JR; Thakur T; Desai P; Jaiswal MK; Sears N; Cosgriff-Hernandez E; Kaunas R; Gaharwar AK Bioactive Nanoengineered Hydrogels for Bone Tissue Engineering: A Growth-Factor-Free Approach. ACS Nano 2015, 9 (3), 3109–3118. [PubMed: 25674809]

(10). Hobzova R; Hrib J; Sirc J; Karpushkin E; Michalek J; Janouskova O; Gatenholm P Embedding of Bacterial Cellulose Nanofibers within PHEMA Hydrogel Matrices: Tunable Stiffness Composites with Potential for Biomedical Applications. J. Nanomater 2018, 2018, 1–11.

(11). Stowers RS; Allen SC; Suggs LJ Dynamic Phototuning of 3D Hydrogel Stiffness. Proc. Natl. Acad. Sci. U. S. A 2015, 112 (7), 1953–1958. [PubMed: 25646417]

(12). Blaeser A; Duarte Campos DF; Puster U; Richtering W; Stevens MM; Fischer H Controlling Shear Stress in 3D Bioprinting Is a Key Factor to Balance Printing Resolution and Stem Cell Integrity. Adv. Healthcare Mater 2016, 5 (3), 326–333.

(13). Pei Y; Ye D; Zhao Q; Wang X; Zhang C; Huang W; Zhang N; Liu S; Zhang L Effectively Promoting Wound Healing with Cellulose/Gelatin Sponges Constructed Directly from a Cellulose Solution. J. Mater. Chem. B 2015, 3 (38), 7518–7528. [PubMed: 32262635]

(14). Rees A; Powell LC; Chinga-Carrasco G; Gethin DT; Syverud K; Hill KE; Thomas DW 3D Bioprinting of Carboxymethylated-Periodate Oxidized Nanocellulose Constructs for Wound Dressing Applications. BioMed Res. Int 2015, 2015, 1–7.

(15). Shin SR; Zihlmann C; Akbari M; Assawes P; Cheung L; Zhang K; Manoharan V; Zhang YS; Yüksekkaya M; Wan KT; Nikkhah M; Dokmeci MR; Tang XS; Khademhosseini A Reduced Graphene Oxide-GelMA Hybrid Hydrogels as Scaffolds for Cardiac Tissue Engineering. Small 2016, 12, 3677–3689. [PubMed: 27254107]

(16). Ku SH; Lee SH; Park CB Synergic Effects of Nanofiber Alignment and Electroactivity on Myoblast Differentiation. Biomaterials 2012, 33 (26), 6098–6104. [PubMed: 22681977]

(17). Rowlands AS; Cooper-White JJ Directing Phenotype of Vascular Smooth Muscle Cells Using Electrically Stimulated Conducting Polymer. Biomaterials 2008, 29 (34), 4510–4520. [PubMed: 18789820]

(18). Zhu W; Ye T; Lee SJ; Cui H; Miao S; Zhou X; Shuai D; Zhang LG Enhanced Neural Stem Cell Functions in Conductive Annealed Carbon Nanofibrous Scaffolds with Electrical Stimulation. Nanomedicine 2017, 14 (7), 2485–2494. [PubMed: 28552650]

(19). Dvir T; Timko BP; Brigham MD; Naik SR; Karajanagi SS; Levy O; Jin H; Parker KK; Langer R; Kohane DS Nanowired Three-Dimensional Cardiac Patches. Nat. Nanotechnol 2011, 6 (11), 720–725. [PubMed: 21946708]

(20). Koppes AN; Keating KW; McGregor AL; Koppes RA; Kearns KR; Ziemba AM; McKay CA; Zuidema JM; Rivet CJ; Gilbert RJ; Thompson DM Robust Neurite Extension Following Exogenous Electrical Stimulation within Single Walled Carbon Nanotube-Composite Hydrogels. Acta Biomater. 2016, 39, 34–43. [PubMed: 27167609]

(21). Onoe H; Okitsu T; Itou A; Kato-Negishi M; Gojo R; Kiriya D; Sato K; Miura S; Iwanaga S; Kuribayashi-Shigetomi K; Matsunaga YT; Shimoyama Y; Takeuchi S Metre-Long Cell-Laden Microfibres Exhibit Tissue Morphologies and Functions. Nat. Mater 2013, 12 (6), 584–590. [PubMed: 23542870]

(22). Zhu K; Shin SR; van Kempen T; Li YC; Ponraj V; Nasajpour A; Mandla S; Hu N; Liu X; Leijten J; Lin YD; Hussain MA; Zhang YS; Tamayol A; Khademhosseini A Gold Nanocomposite Bioink for Printing 3D Cardiac Constructs. Adv. Funct. Mater 2017, 27 (12), 1605352. [PubMed: 30319321]

(23). Shin SR; Farzad R; Tamayol A; Manoharan V; Mostafalu P; Zhang YS; Akbari M; Jung SM; Kim D; Comotto M; Annabi N; Al-Hazmi FE; Dokmeci MR; Khademhosseini A A Bioactive Carbon Nanotube-Based Ink for Printing 2D and 3D Flexible Electronics. Adv. Mater 2016, 28 (17), 3280–3289. [PubMed: 26915715]

(24). Huang C-T; Kumar Shrestha L; Ariga K; Hsu S A Graphene–Polyurethane Composite Hydrogel as a Potential Bioink for 3D Bioprinting and Differentiation of Neural Stem Cells. J. Mater. Chem. B 2017, 5, 8854–8864. [PubMed: 32264279]

(25). Xia Q; Ray PC; Yu H; Hwang H-M; Fu PP Mechanisms of Nanotoxicity: Generation of Reactive Oxygen Species. J. Food Drug Anal 2014, 22 (1), 64–75. [PubMed: 24673904]

(26). Hinton TJ; Jallerat Q; Palchesko RN; Park JH; Grodzicki MS; Shue H-J; Ramadan MH; Hudson AR; Feinberg AW Three-Dimensional Printing of Complex Biological Structures by Freeform Reversible Embedding of Suspended Hydrogels. Sci. Adv 2015, 1 (9), No. e1500758. [PubMed: 26601312]

(27). Bhattacharjee T; Gil CJ; Marshall SL; Urueña JM; O'Bryan CS; Carstens M; Keselowsky B; Palmer GD; Ghivizzani S; Gibbs CP; Sawyer WG; Angelini TE Liquid-like Solids Support Cells in 3D. ACS Biomater. Sci. Eng 2016, 2 (10), 1787–1795. [PubMed: 33440476]

(28). Taubenberger AV; Woodruff MA; Bai H; Muller DJ; Hutmacher DW The Effect of Unlocking RGD-Motifs in Collagen I on Pre-Osteoblast Adhesion and Differentiation. Biomaterials 2010, 31 (10), 2827–2835. [PubMed: 20053443]

(29). Grinnell F Fibroblast Biology in Three-Dimensional Collagen Matrices. Trends Cell Biol. 2003, 13 (5), 264–269. [PubMed: 12742170]

(30). Nocera AD; Comín R; Salvatierra NA; Cid MP Development of 3D Printed Fibrillar Collagen Scaffold for Tissue Engineering. Biomed. Microdevices 2018, 20 (2), 1–13.

(31). Koo YW; Choi EJ; Lee JY; Kim HJ; Kim GH; Do SH 3D Printed Cell-Laden Collagen and Hybrid Scaffolds for in Vivo Articular Cartilage Tissue Regeneration. J. Ind. Eng. Chem 2018, 66, 343–355.

(32). Spencer A; Primbetova A; Koppes AN; Koppes R; Fenniri H; Annabi N Electroconductive Gelatin Methacryloyl-PEDOT:PSS Composite Hydrogels: Design, Synthesis, and Properties. ACS Biomater. Sci. Eng 2018, 4 (5), 1558–1567. [PubMed: 33445313]

(33). Klotz BJ; Gawlitta D; Rosenberg AJWP; Malda J; Melchels FPW Gelatin-Methacryloyl Hydrogels: Towards Biofabrication-Based Tissue Repair. Trends Biotechnol. 2016, 34 (5), 394–407. [PubMed: 26867787]

(34). Yue K; Trujillo-De Santiago G; Alvarez MM; Tamayol A; Annabi N; Khademhosseini A Synthesis, Properties, and Biomedical Applications of Gelatin Methacryloyl (GelMA) Hydrogels. Biomaterials 2015, 73, 254–271. [PubMed: 26414409]

(35). Shirzaei Sani E; Kheirkhah A; Rana D; Sun Z; Foulsham W; Sheikhi A; Khademhosseini A; Dana R; Annabi N Sutureless Repair of Corneal Injuries Using Naturally Derived Bioadhesive Hydrogels. Sci. Adv 2019, 5 (3), eaav1281. [PubMed: 30906864]

(36). Zhao X; Sun X; Yildirimer L; Lang Q; Lin ZY; Zheng R; Zhang Y; Cui W; Annabi N; Khademhosseini A Cell Infiltrative Hydrogel Fibrous Scaffolds for Accelerated Wound Healing. Acta Biomater. 2017, 49, 66–77. [PubMed: 27826004]

(37). Tasoglu S; Yu CH; Gungordu HI; Guven S; Vural T; Demirci U Guided and Magnetic Self-Assembly of Tunable Magnetoceptive Gels. Nat. Commun 2014, 5, 4702. [PubMed: 25175148]

(38). Shirzaei Sani E; Portillo-Lara R; Spencer A; Yu W; Geilich BM; Noshadi I; Webster TJ; Annabi N Engineering Adhesive and Antimicrobial Hyaluronic Acid/Elastin-like Polypeptide Hybrid

Hydrogels for Tissue Engineering Applications. ACS Biomater. Sci. Eng 2018, 4 (7), 2528–2540. [PubMed: 33435116]

(39). Soucy JR; Shirzaei Sani E; Portillo Lara R; Diaz D; Dias F; Weiss AS; Koppes AN; Koppes RA; Annabi N Photo-crosslinkable Gelatin/Tropoelastin Hydrogel Adhesives for Peripheral Nerve Repair. Tissue Eng., Part A 2018, 24 (17–18), 1393–1405. [PubMed: 29580168]

(40). Gornall JL; Terentjev EM Helix–Coil Transition of Gelatin: Helical Morphology and Stability. Soft Matter 2008, 4 (3), 544–549. [PubMed: 32907218]

(41). Ghosh S; Rasmusson J; Inganäs O Supramolecular Self-Assembly for Enhanced Conductivity in Conjugated Polymer Blends: Ionic Crosslinking in Blends of Poly (3,4-Ethylenedioxythiophene)-Poly(Styrenesulfonate) and Poly(Vinylpyrrolidone). Adv. Mater 1998, 10 (14), 1097–1099.

(42). Colosi C; Shin SR; Manoharan V; Massa S; Costantini M; Barbetta A; Dokmeci MR; Dentini M; Khademhosseini A Microfluidic Bioprinting of Heterogeneous 3D Tissue Constructs Using Low-Viscosity Bioink. Adv. Mater 2016, 28, 677–684. [PubMed: 26606883]

(43). Walker BW; Portillo Lara R; Mogadam E; Hsiang Yu C; Kimball W; Annabi N Rational Design of Microfabricated Electroconductive Hydrogels for Biomedical Applications. Prog. Polym. Sci 2019, 92, 135–157. [PubMed: 32831422]

(44). Annabi N; Shin SR; Tamayol A; Miscuglio M; Bakooshli MA; Assmann A; Mostafalu P; Sun JY; Mithieux S; Cheung L; Tang X; Weiss AS; Khademhosseini A Highly Elastic and Conductive Human-Based Protein Hybrid Hydrogels. Adv. Mater 2016, 28 (1), 40–49. [PubMed: 26551969]

(45). Hennink WE; van Nostrum CF Novel Crosslinking Methods to Design Hydrogels. Adv. Drug Delivery Rev 2012, 64, 223–236.

(46). Bhana B; Iyer RK; Chen WLK; Zhao R; Sider KL; Likhitpanichkul M; Simmons CA; Radisic M Influence of Substrate Stiffness on the Phenotype of Heart Cells. Biotechnol. Bioeng 2010, 105 (6), 1148–1160. [PubMed: 20014437]

(47). Gilbert PM; Havenstrite KL; Magnusson KEG; Sacco A; Leonardi N. a.; Kraft P; Nguyen NK; Thrun S; Lutolf MP; Blau HM Substrate Elasticity Regulates Skeletal Muscle Stem Cell Self-Renewal in Culture. Science (Washington, DC, U. S.) 2010, 329 (5995), 1078–1081.

(48). Wisse E; Govaert LE; Meijer HEH; Meijer EW Unusual Tuning of Mechanical Properties of Thermoplastic Elastomers Using Supramolecular Fillers. Macromolecules 2006, 39 (21), 7425–7432.

(49). Jordan SW; Rutz AL; Secor EB; Shah RN; Jakus AE; Hersam MC Three-Dimensional Printing of High-Content Graphene Scaffolds for Electronic and Biomedical Applications. ACS Nano 2015, 9 (4), 4636–4648. [PubMed: 25858670]

(50). Lee SJ; Zhu W; Nowicki M; Lee G; Heo DN; Kim J; Zuo YY; Zhang LG 3D Printing Nano Conductive Multi-Walled Carbon Nanotube Scaffolds for Nerve Regeneration. J. Neural Eng 2018, 15 (1), 016018. [PubMed: 29064377]

(51). Engler AJ; Carag-Krieger C; Johnson CP; Raab M; Tang H-Y; Speicher DW; Sanger JW; Sanger JM; Discher DE Embryonic Cardiomyocytes Beat Best on a Matrix with Heart-like Elasticity: Scar-like Rigidity Inhibits Beating. J. Cell Sci 2008, 121 (22), 3794–3802. [PubMed: 18957515]

(52). Discher DE; Janmey P; Wang Y Tissue Cells Feel and Respond to the Stiffness of Their Substrate. Science (Washington, DC, U. S.) 2005, 310 (5751), 1139–1143.

(53). Kamata H; Akagi Y; Kayasuga-Kariya Y; Chung U; Sakai T Nonswellable" Hydrogel Without Mechanical Hysteresis. Science (Washington, DC, U. S.) 2014, 343 (6173), 873–875.

(54). Xu C; Lee W; Dai G; Hong Y Highly Elastic Biodegradable Single-Network Hydrogel for Cell Printing. ACS Appl. Mater. Interfaces 2018, 10 (12), 9969–9979. [PubMed: 29451384]

(55). Odent J; Wallin TJ; Pan W; Kruemplestaedter K; Shepherd RF; Giannelis EP Highly Elastic, Transparent, and Conductive 3D-Printed Ionic Composite Hydrogels. Adv. Funct. Mater 2017, 27 (33), 1701807.

(56). Dubbin K; Hori Y; Lewis KK; Heilshorn SC Dual-Stage Crosslinking of a Gel-Phase Bioink Improves Cell Viability and Homogeneity for 3D Bioprinting. Adv. Healthcare Mater 2016, 5 (19), 2488–2492.

(57). Bhattacharjee T; Zehnder SM; Rowe KG; Jain S; Nixon RM; Sawyer WG; Angelini TE Writing in the Granular Gel Medium. Sci. Adv 2015, 1 (8), No. e1500655. [PubMed: 26601274]

(58). Burke NJ; Burrows AD; Mahon MF; Teat SJ Incorporation of Sulfonate Dyes into Hydrogen-Bonded Networks. CrystEngComm 2004, 6 (71), 429–436.

(59). Kang H-W; Lee SJ; Ko IK; Kengla C; Yoo JJ; Atala AA 3D Bioprinting System to Produce Human-Scale Tissue Constructs with Structural Integrity. Nat. Biotechnol 2016, 34 (3), 312–319. [PubMed: 26878319]

(60). Lozano R; Stevens L; Thompson BC; Gilmore KJ; Gorkin R; Stewart EM; In het Panhuis M; Romero-Ortega M; Wallace GG 3D Printing of Layered Brain-like Structures Using Peptide Modified Gellan Gum Substrates. Biomaterials 2015, 67, 264–273. [PubMed: 26231917]

(61). Sarker MD; Naghieh S; Sharma NK; Chen X 3D Biofabrication of Vascular Networks for Tissue Regeneration: A Report on Recent Advances. J. Pharm. Anal 2018, 8 (5), 277–296. [PubMed: 30345141]

(62). Cooper ST; Maxwell AL; Kizana E; Ghoddusi M; Hardeman EC; Alexander IE; Allen DG; North KN C2C12 Co-Culture on a Fibroblast Substratum Enables Sustained Survival of Contractile, Highly Differentiated Myotubes with Peripheral Nuclei and Adult Fast Myosin Expression. Cell Motil. Cytoskeleton 2004, 58 (3), 200–211. [PubMed: 15146538]

(63). Li Y; Poon CT; Li M; Lu TJ; Pingguan-Murphy B; Xu F Chinese-Noodle-Inspired Muscle Myofiber Fabrication. Adv. Funct. Mater 2015, 25 (37), 5999–6008.

(64). Langelaan MLP; Boonen KJM; Rosaria-Chak KY; van der Schaft DWJ; Post MJ; Baaijens FPT Advanced Maturation by Electrical Stimulation: Differences in Response between C2C12 and Primary Muscle Progenitor Cells. J. Tissue Eng. Regener. Med 2011, 5, 529–539.

(65). Kim HJ; Heo DN; Lee YJ; Lee SJ; Kang JY; Lee SH; Kwon IK; Do SH Biological Assessments of Multifunctional Hydrogel-Decorated Implantable Neural Cuff Electrode for Clinical Neurology Application. Sci. Rep 2017, 7 (1), 15245. [PubMed: 29127334]

(66). Salick MR; Napiwocki BN; Sha J; Knight GT; Chindhy SA; Kamp TJ; Ashton RS; Crone WC Micropattern Width Dependent Sarcomere Development in Human ESC-Derived Cardiomyocytes. Biomaterials 2014, 35 (15), 4454–4464. [PubMed: 24582552]

(67). Saini H; Navaei A; Van Putten A; Nikkhah M 3D Cardiac Microtissues Encapsulated with the Co-Culture of Cardiomyocytes and Cardiac Fibroblasts. Adv. Healthcare Mater 2015, 4 (13), 1961–1971.

(68). Noshadi I; Walker BW; Portillo-Lara R; Shirzaei Sani E; Gomes N; Aziziyan MR; Annabi N Engineering Biodegradable and Biocompatible Bio-Ionic Liquid Conjugated Hydrogels with Tunable Conductivity and Mechanical Properties. Sci. Rep 2017, 7 (1), 4345. [PubMed: 28659629]

(69). Wang W; Tan B; Chen J; Bao R; Zhang X; Liang S; Shang Y; Liang W; Cui Y; Fan G; Jia H; Liu W An Injectable Conductive Hydrogel Encapsulating Plasmid DNA-ENOs and ADSCs for Treating Myocardial Infarction. Biomaterials 2018, 160, 69–81. [PubMed: 29396380]

(70). Jang J; Park HJ; Kim SW; Kim H; Park JY; Na SJ; Kim HJ; Park MN; Choi SH; Park SH; Kim SW; Kwon SM; Kim PJ; Cho DW 3D Printed Complex Tissue Construct Using Stem Cell-Laden Decellularized Extracellular Matrix Bioinks for Cardiac Repair. Biomaterials 2017, 112, 264–274. [PubMed: 27770630]

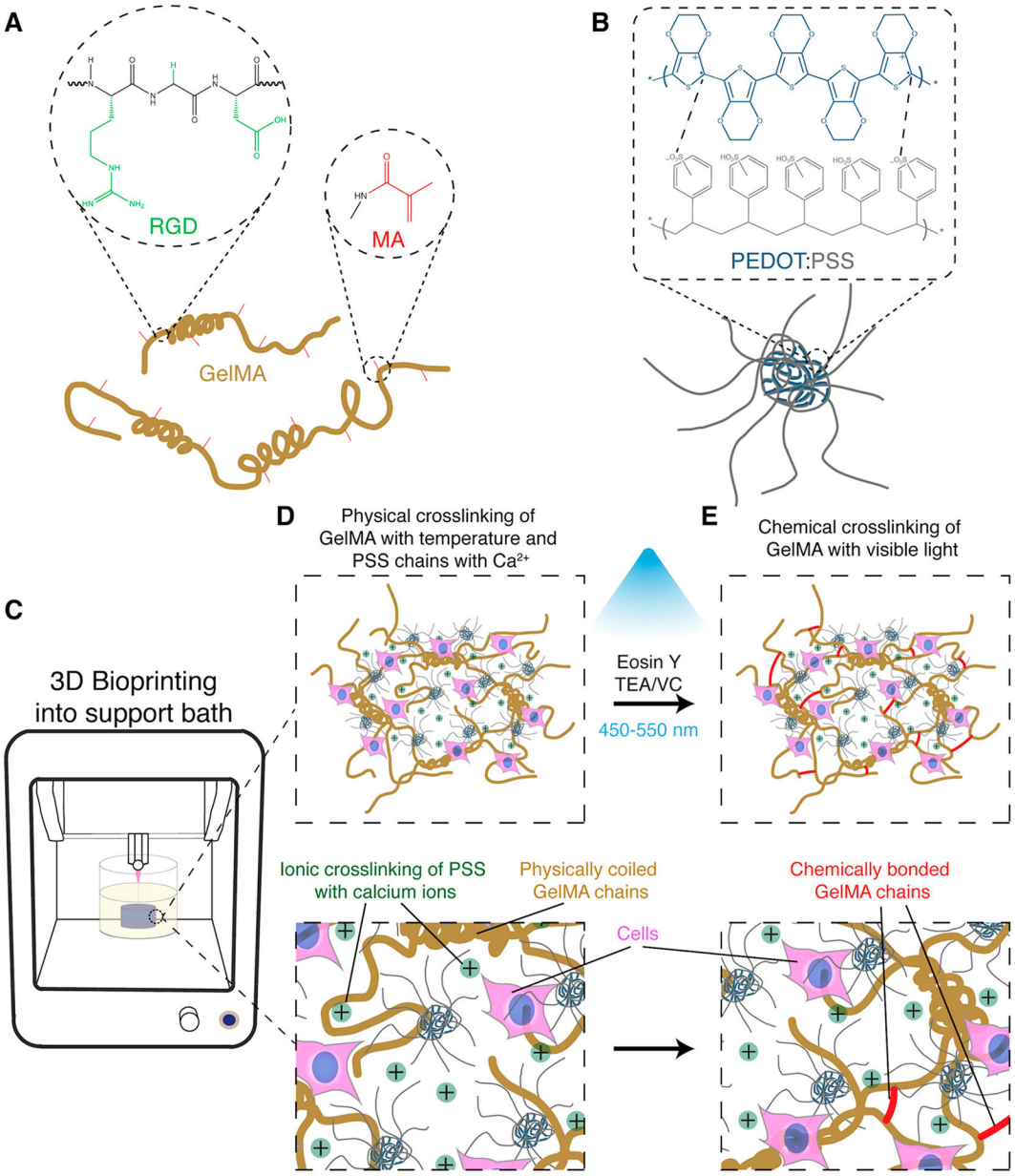


**Figure 1.**

Synthesis of conductive GelMA/PEDOT:PSS bioinks for fabricating cell-laden constructs. (A) GelMA prepolymer chemical structure containing RGD residues to interact with cells and methacryloyl groups to enable photopolymerization in the presence of a photoinitiator and light. (B) PEDOT:PSS chemical structure and schematic of polyelectrolyte complex, showing its coiled spherical structure in aqueous solutions. (C) Schematic of 3D bioprinting of cell-laden GelMA/PEDOT:PSS bioink into a microgel support bath. Cell-laden liquid prepolymer solution was injected into a coagulation bath containing aqueous calcium chloride at 4 °C. (D) Introduction of multivalent cations at low temperature caused the simultaneous unwinding and ionic cross-linking of the PEDOT:PSS and thermally driven

coiling of the GelMA chains. (E) Photo-cross-linking by visible light formed chemical bonds among GelMA chains and further stabilized the structure.

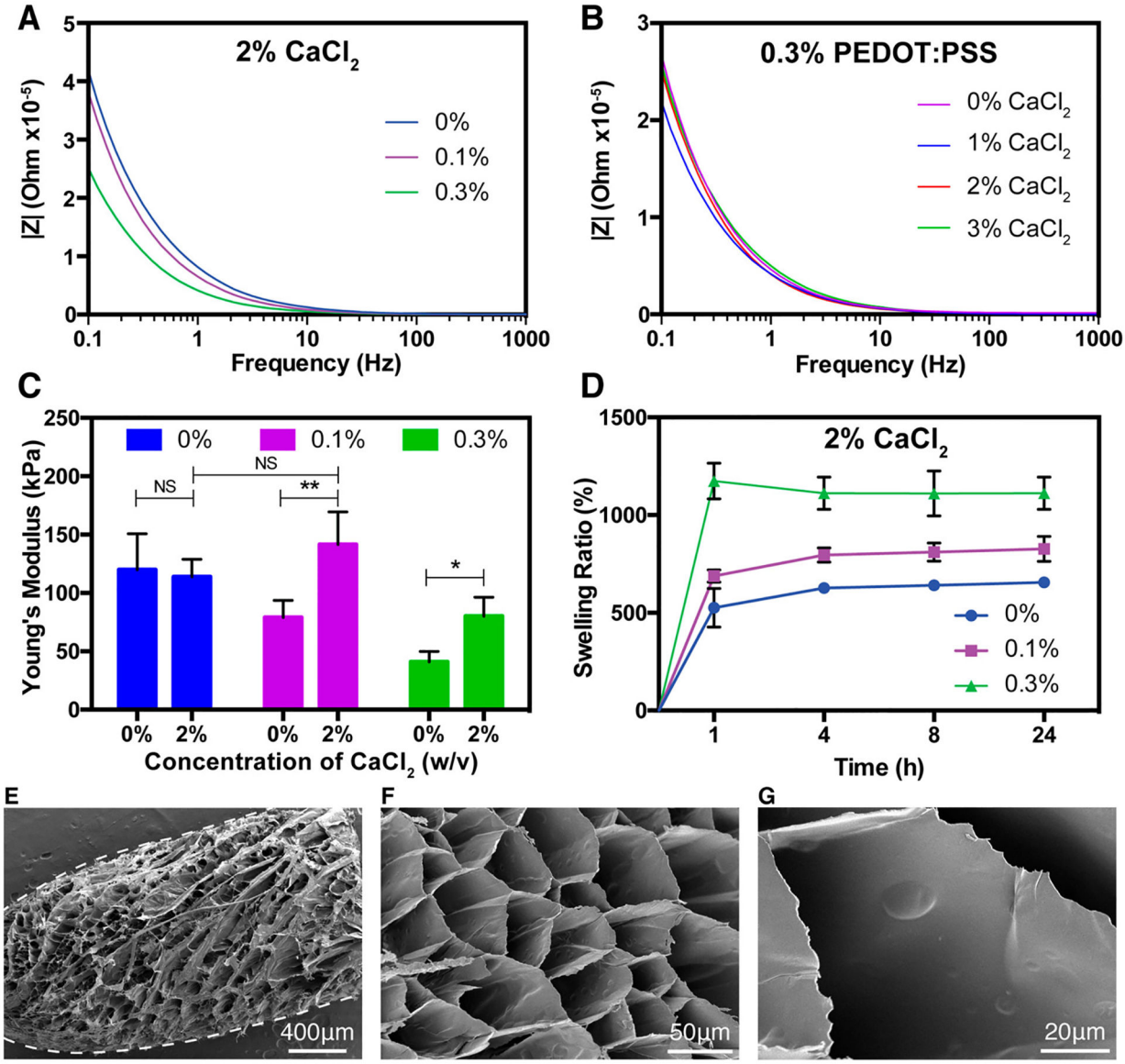


**Figure 2.**

Physical and microstructural characterization of GelMA/PEDOT:PSS hydrogels. (A) EIS spectra of hydrogels cross-linked with 2% (w/v) calcium chloride containing varying concentrations of PEDOT:PSS. (B) EIS spectra of hydrogel samples containing 7% GelMA and 0.3% PEDOT:PSS, cross-linked with varied concentrations of calcium chloride. (C) Young's modulus of hydrogels formed by using various concentrations of PEDOT:PSS, cross-linked with control PBS or 2% calcium chloride solution. (D) Swelling ratio of hydrogels with various concentrations of PEDOT:PSS cross-linked with 2% $CaCl_2$ at different time points. Representative SEM images of (E) a whole fiber after swelling in DI water and lyophilization and (F) cross-section of a fiber formed by wet-spinning procedure with 7% GelMA, 0.3% PEDOT:PSS, and cross-linked with 2% $CaCl_2$. (G) High magnification representative SEM image of a hydrogel showing the absence of large aggregated particles. (Data plotted as mean ± SD, * = $p < 0.05$; ** = $p < 0.01$).

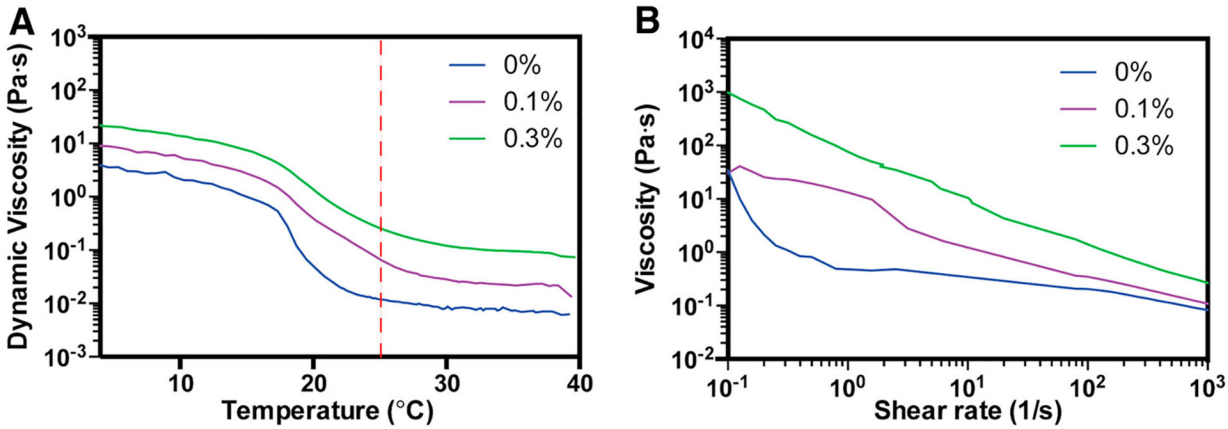


**Figure 3.**

Rheological characterization of GelMA/PEDOT:PSS bioinks. (A) Dynamic viscosity of GelMA/PEDOT:PSS bioinks in the temperature range from 4 to 40 °C, showing higher viscosity of inks containing PEDOT:PSS at all temperatures, and the same trend in viscosity change with temperature. Red-dotted line is drawn at 25 °C and indicates the temperature at which the bioinks were printed. (B) Strain sweeps of GelMA/PEDOT:PSS bioinks demonstrating their shear-thinning properties, and the enhancement of this property with the addition of PEDOT:PSS.

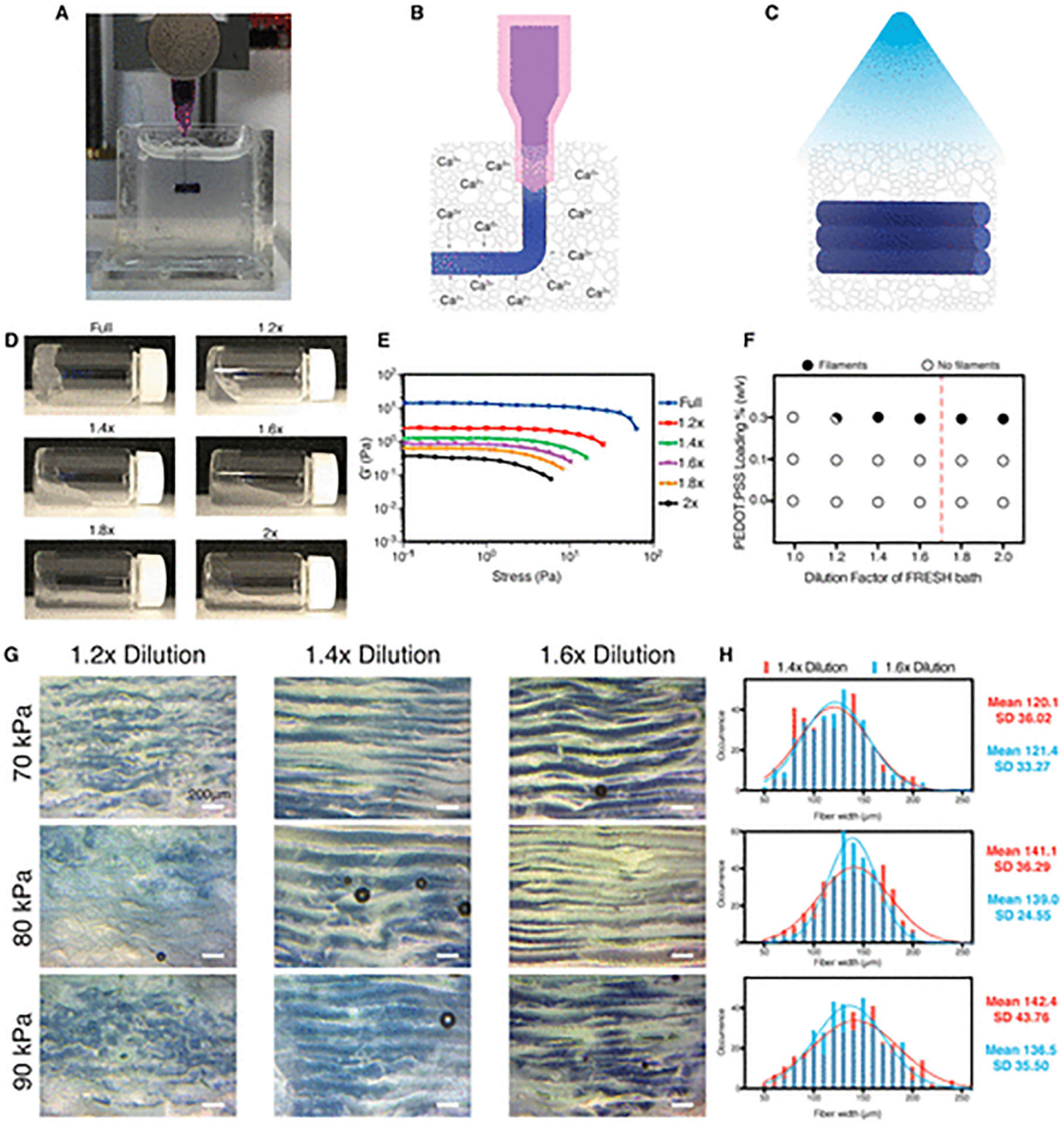


**Figure 4.**

Optimization of 3D printing of GelMA/PEDOT:PSS hydrogel in reduced packing support bath. (A) Photograph of printing the GelMA/PEDOT:PSS bioink into the gelatin microgel support bath containing calcium chloride. (B) Schematic showing how the particles are surrounding the extruded filaments and support the filaments as they are extruded. Calcium ions flux into the filaments as they are extruded, cross-linking the PSS chains. (C) Exposing the printed structures to light is necessary to cross-link the GelMA chains and stabilize the mechanical integrity of the printed structure. (D) Inverted vial photographs show the flow behavior of the support baths at different dilutions. (E) Oscillatory stress sweeps of the support baths show that the storage modulus is steady until a threshold stress, at which the fluids yield. This threshold reduced as the packing of the particles is reduced. (F) Graph

demonstrating the formulations of bioink and support bath that resulted in clear filaments. (G) Lateral cross-section phase contrast images of structures printed with bioink containing 7% GelMA and 0.3% PEDOT:PSS into support baths with varied packing and at different applied pressures. (H) Histograms showing the Gaussian-like distribution of fiber diameters at 1.4× and 1.6× dilutions.

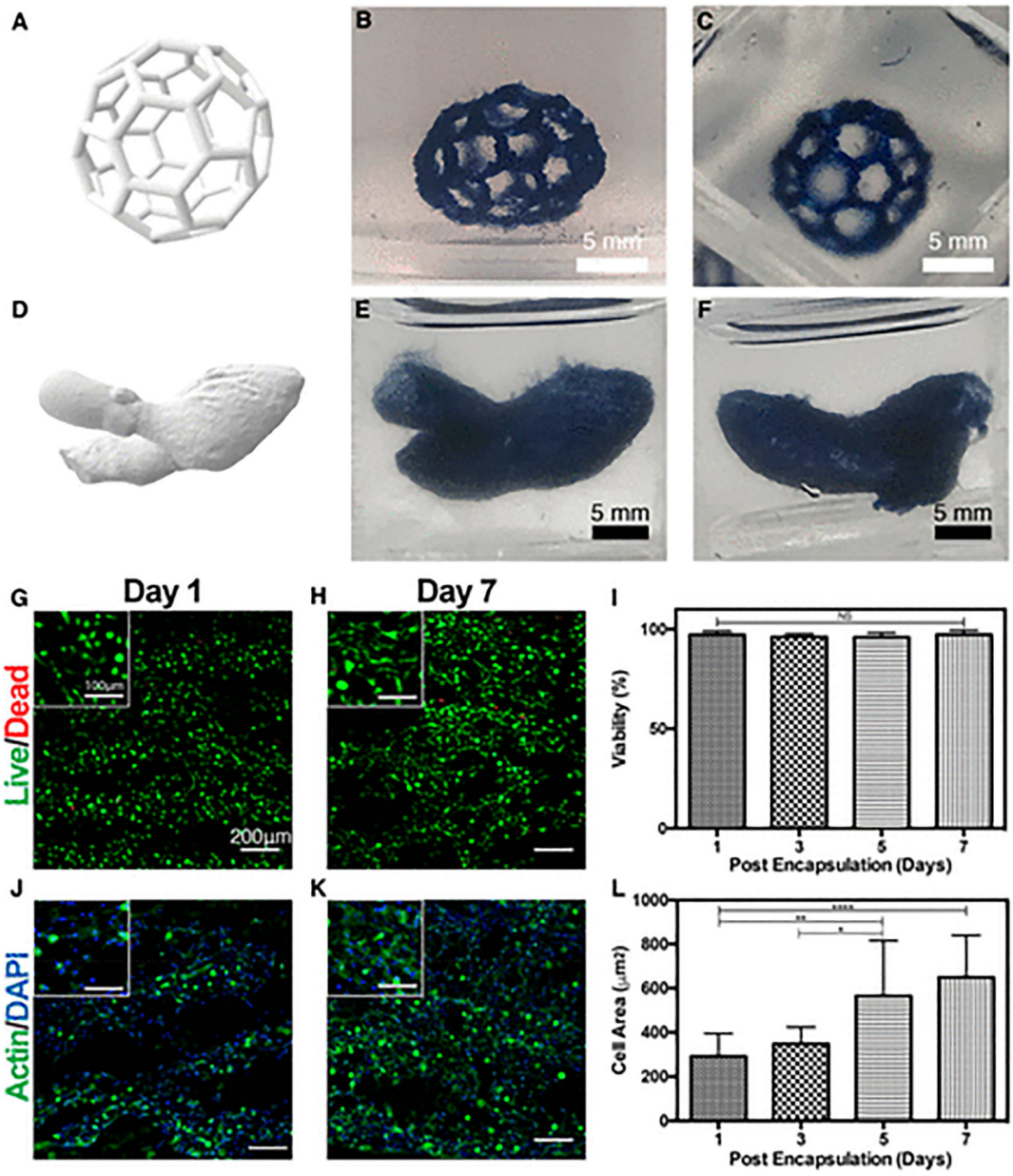


**Figure 5.**

3D Bioprinting of complex structures using the synthesized GelMA/PEDOT:PSS bioink. (A) 3D rendering of a complex buckyball structure used for 3D printing. (B) Side view of the 3D printed buckyball structure printed using the GelMA/PEDOT:PSS bioink. (C) Top view of the 3D printed buckyball structure. (D) 3D rendering of a left ventricle complete with the ascending aorta used for printing a cardiac structure. (E) Front view of the 3D printed ventricle structure with the GelMA/PEDOT:PSS bioink. (F) Back view of the 3D printed ventricle structure. Representative live/dead stained images of C2C12 cells encapsulated in 3D printed cylindrical ring structures at (G) day 1 and (H) day 7. (I) Quantification of cell viability from live/dead images. Representative actin/DAPI stained images of C2C12 cells encapsulated in the 3D printed structure at (J) day 1 and (K) day 7. Dark areas in the

image indicate portions where cells were out of the plane of focus and were removed as background. (L) Quantification of cell spreading from actin/DAPI images. (Data plotted as mean ± SD, * = $p < 0.05$; ** = $p < 0.01$; **** = $p < 0.0001$).

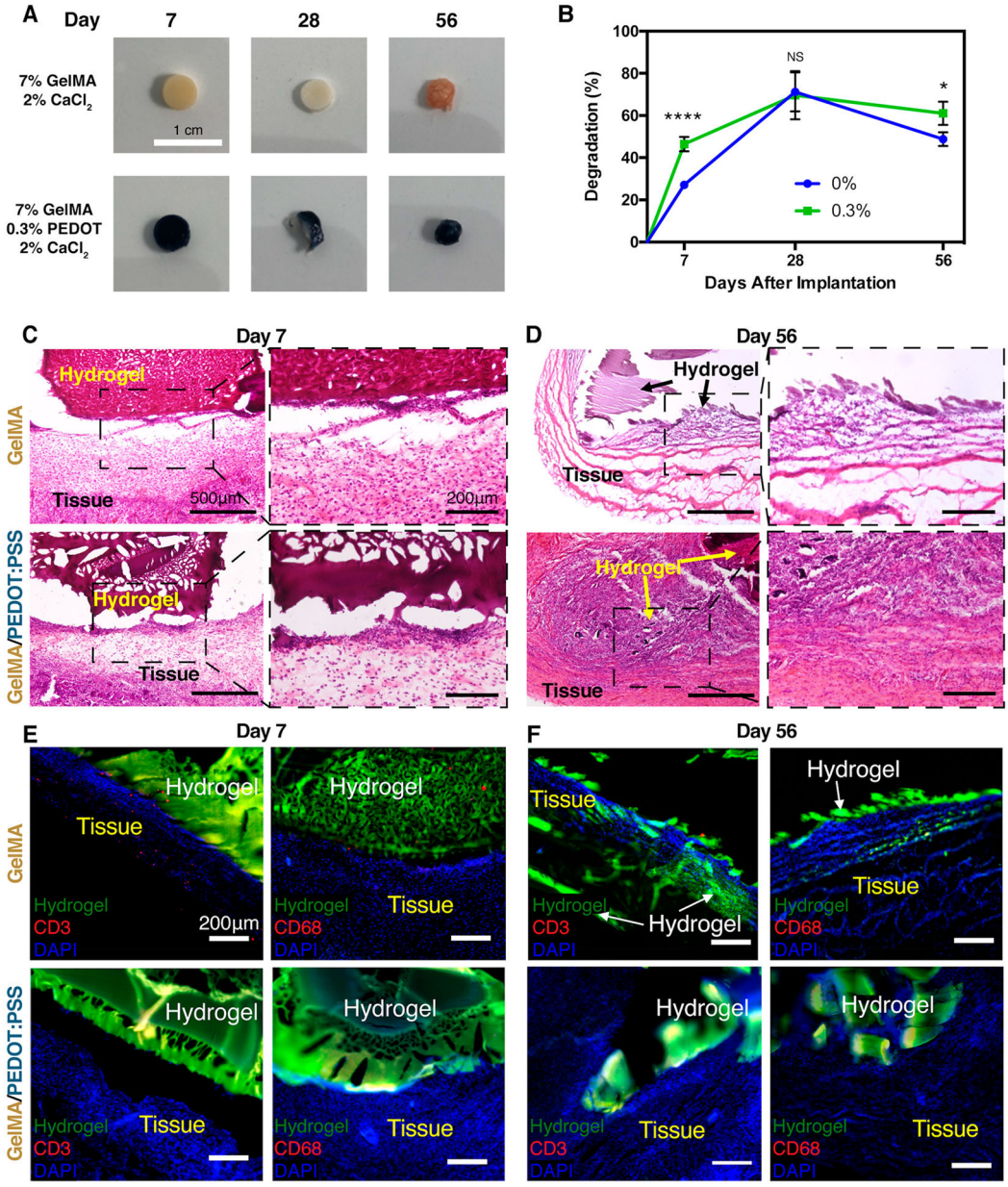


**Figure 6.**

In vivo biodegradation and biocompatibility of subcutaneously implanted GelMA/PEDOT:PSS and GelMA hydrogels in rats. (A) Photographs of cylindrical hydrogel samples at various post implantation times. (B) In vivo biodegradation by wt % for pure GelMA hydrogel and GelMA/PEDOT:PSS hydrogel formed by using 0.3% PEDOT:PSS. (* = $p < 0.05$; **** = $p < 0.0001$). Representative H&E stained images from the cross sections of GelMA (top) and GelMA/PEDOT:PSS (bottom) cross-linked with 2% $CaCl_2$ explanted at (C) day 7 and (D) day 56. (E) Immunofluorescent analysis of subcutaneously implanted GelMA and GelMA/PEDOT:PSS hydrogels showed minor local lymphocyte infiltration (CD3) and no significant macrophage infiltration (CD68) at 7 days post implantation. (F) At 56 days post implantation, the lymphocytes had cleared from the region of implantation

for GelMA hydrogels, and no macrophages had infiltrated the hydrogel or surrounding tissue. For implanted GelMA/PEDOT:PSS hydrogels, lymphocytes and macrophages were still absent from the implantation space at day 56.